Structural Study of Prolinium Fumaric Acid Zwitterionic Cocrystals Focus on Hydrogen-Bonding Pattern Involving Zwitterionic (Ionic) heterosynthons

ARTICLE *in* CRYSTAL GROWTH & DESIGN · JANUARY 2013

Impact Factor: 4.89

2 AUTHORS:

Anaelle Tilborg

University of Namur / UCL (Louvain-la-Neuve)

19 PUBLICATIONS **40** CITATIONS

SEE PROFILE

Johan Wouters

University of Namur

280 PUBLICATIONS **3,471** CITATIONS

SEE PROFILE

CRYSTAL GROWTH & DESIGN

Article

Structural Study of Prolinium/Fumaric Acid Zwitterionic Cocrystals: Focus on Hydrogen-Bonding Pattern Involving Zwitterionic (Ionic) Heterosynthons

Anaëlle Tilborg,[†] Tom Leyssens,[‡] Bernadette Norberg,[†] and Johan Wouters*[,†]

[†]Unité de Chimie Physique Théorique et Structurale, Department of Chemistry, University of Namur, 61, rue de Bruxelles, B-5000 Namur, Belgium

[‡]IMCN, MOST, UCL, 1, Place Louis Pasteur, B-1348 Louvain-la-Neuve, Belgium

Supporting Information

ABSTRACT: Pharmaceutical compounds are mostly developed as solid dosage forms containing a single crystal form. This implies that the selection of a particular crystal state for a given molecule is an important step for further clinical outlooks. Different methods can be used in the case of polymorphism issues at the time of optimal phase selection. One of the promising techniques developed these last few years is cocrystallization. In this context, proline (pyrrolidine-2-carboxylic acid) is considered in the present work. Cocrystals of proline and fumaric acid (*E*-butenedioic acid) are mainly analyzed by powder and single-crystal X-ray diffraction (PXRD and SCXRD, respectively). At first, the cocrystallization conditions are optimized by grinding (dry grinding), a green method for cocrystals screening and synthesis. Under specific conditions, single crystals of a 2:1 L-proline−fumaric acid racemic zwitterionic cocrystal have been obtained, an outcome confirmed by crystallographic analysis. Enantiomeric cocrystal form was obtained starting from D-proline. With the racemic compound (DL-proline), a three-component cocrystal is formed, the 1:1:1 L-proline−D-proline−fumaric acid cocrystal. Interestingly, this latter seems to be obtained using two distinct synthetic ways. Calorimetric measurements have been performed in order to establish the binary-phase diagram of the L-proline−fumaric acid cocrystal. Structural comparison with related structures from the Cambridge Structural Database revealed similarities in the crystalline network and introduced a systematic and detailed analysis of hydrogen bond interactions in zwitterionic cocrystalline structures involving proline.

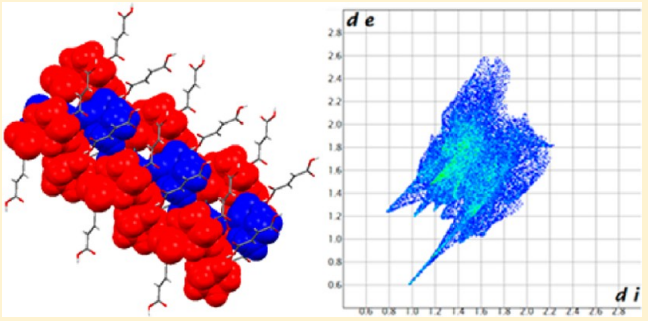

INTRODUCTION

Different methods can be used to deal with problems when a compound of therapeutic interest (active pharmaceutical ingredient or API) presents unsuitable physicochemical properties (e.g., melting point too low for the further development; inappropriate dissolution rate or solubility itself) or exhibits different polymorphic forms that interconvert at ambient temperature with only one being therapeutically appropriate.[1−3]

To improve physicochemical properties (e.g., solubility, dissolution rate), formulation scientists turn to various basic approaches, such as salt formation, or solid-state approaches, such as amorphization or metastable phase formation.[1,4]

Although the formation of salts is an excellent means of altering the physicochemical properties of an API,[5] it requires at least one ionizable center. Furthermore, the number of pharmaceutically acceptable salt formers is relatively small.[6,7]

When the pharmaceutical compound of interest does not present ionizable functions and when the formation of amorphous or metastable phase is not a viable option, formation of pharmaceutical cocrystal is a well-adapted method for improving physicochemical properties of APIs.[8,9] Indeed, cocrystallization is regarded as one of the promising approaches in the field of pharmaceutical solid-state chemistry,[4,10−12] and recent studies highlight the advantages of using cocrystallization as a mean to optimize physicochemical properties or avoid the appearance of unwanted polymorphic forms.[8,13−15]

Our interest in proline (Pro) lies in the fact that, besides being one of the natural α-amino acids composing proteins, this molecule has already been implicated in cocrystals and hence could be a valuable cocrystal former (considering the ease of forming cocrystal with the selected partner of interest).[16−19] Its precise role to stabilize the cocrystals and a detailed understanding at the molecular level of the interactions involved in these multicomponent molecular complexes deserve attention. Recent studies on the mediator role of proline in aldol organic catalysis and amplification of enantiomeric excess[20−22] further justify solid-state studies of this molecule, in the framework of preparation of solid−solid

Received: January 15, 2013
Revised: May 10, 2013
Published: May 14, 2013

reactions. In that context, the present study describing the preparation of original cocrystals of proline provides the structural basis for the role that it can play within solid state molecular complexes and opens perspectives for the further use of this compound as a potential cocrystal former when combined with molecules of pharmaceutical interest.

EXPERIMENTAL SECTION

Materials. L-Proline, D-proline, DL-proline (≥99% chemical purity), D-prolinamide, and fumaric acid (99%) (Scheme 1) were sourced from Sigma-Aldrich (Steinheim, Germany) and used as received. All compounds were initially characterized by X-ray powder diffraction. Solvents used (essentially 2-propanol from Acros Organic, Geel, Belgium) are commercially available and were used with no further purification.

Scheme 1. Semi-Developed Formulae of L-Prolinium ((2*S*)-Pyrrolidinium-2-carboxylate), D-Prolinium ((2*R*)-Pyrrolidinium-2-carboxylate), Fumaric Acid (*E*-Butenedioic Acid), and D-Prolinamide ((2*R*)-2-Carbamoylpyrrolidinium) (Zwitterionic or Charged Forms)

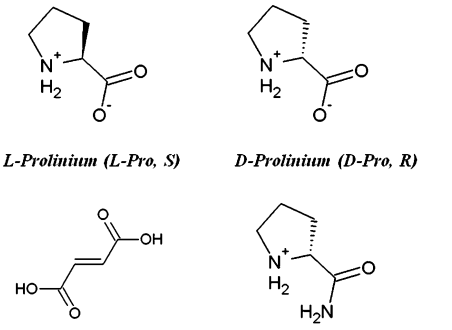

Grinding Experiments. Dry grinding was performed with a Retsch MM 400 Mixer Mill, equipped with two grinding jars in which five 2-mL Eppendorf tubes can be installed and eight to ten stainless steel grinding balls (1 mm diameter) in a sample.

Powder X-ray Diffraction (PXRD). Powder X-ray diffraction data were collected on a PANalytical Bragg–Brentano-geometry diffractometer, using Ni-filtered Cu Kα radiation (λ = 1.54179 Å) at 40 kV and 40 mA with a X'Celerator detector. Each sample was analyzed between 4 and 50° in 2θ with a step size of ca. 0.0167° and a total scan time of 3 min 48 s.

Single-Crystal X-ray Diffraction (SCXRD). Single crystal X-ray diffraction was performed on a Gemini Ultra R system (4-circle kappa platform, Ruby CCD detector) using Mo Kα (λ = 0.71073 Å) radiation. Selected crystals were mounted on the tip of a quartz pin using cyanoacrylate (Commercial glue). Cell parameters were estimated from a pre-experiment run, and full data sets were collected at room temperature. Structures were solved by direct methods with the SHELXS-97 program and then refined on F2 using SHELXL-97 software.[21] Non-hydrogen atoms were anisotropically refined and the hydrogen atoms (not implicated in H-bonds) in the riding mode with isotropic temperature factors fixed at 1.2 times *U*(eq) of the parent atoms (1.5 times for methyl groups). Hydrogen atoms implicated in H-bonds were localized by Fourier difference maps (ΔF). CCDC 919225, 918731, 918730, and 918411 entries contain the supplementary crystallographic data for this paper and can be obtained free of charge via www.ccdc.cam.ac.uk/conts/retrieving.html (or from the Cambridge Crystallographic Data Center, 12, Union Road, Cambridge CB21EZ, UK; fax: +44-1223-336033; or deposit@ccdc.cam.ac.uk). Disordered non-H atoms in prolinium and fumaric acid have been modeled over two sites of different occupancy, when necessary. Details of data collection and structure refinement are listed in Table 1, and selected geometrical parameters (including H-bonds and graph-sets) are presented in Table 2. For the four crystals studied here, CIF files are presented as Supporting Information.

Differential Scanning Calorimetry (DSC). Coupled DSC and TG analysis was performed using a NETZSCH TG/DSC STA 449C instrument. Solid samples (mass of ca. 3 mg) were placed in aluminum sample pans with sealed lids. Helium was used as purge gas with a flow rate of 40 mL/min, and the heating rate was fixed at 20 K/min, between 30 and 250 °C. The data treatment was performed with the Netzsch-TA Proteus Software v.4.8.4.

Calculated Morphology. Simulated morphology has been calculated from the structural data with the geometric method from Bravais, Friedel, Donnay and Harker (BFDH)[23] and was determined with Mercury v. 3.0 software,[24] a comprehensive range of tools for structure visualization and exploration of crystal packing.

Graphical Display and Simulation of PXRD Diffractograms. Images from structural data and calculated patterns have been carried out with Mercury v. 3.0 software.[24]

Search in the Cambridge Structural DataBase (CSD). A statistical study in CSD 2012 (version 5.33, last updated Augustus 2012) for prolinium was performed using the ConQuest program to search and retrieve information,[25] with a two-dimensional representation of the zwitterion as search group. No other restrictions (such as *R*-factor or disorder) were applied during the search. In total, 151 structures were retrieved and 15 structures (containing all a nonmetallic coformer) were fully analyzed with Mercury v. 3.0 software,[24] and VISTA v. 2.3.8 software,[26] an interactive analytical and statistical program.

Conformational Analysis by Quantum Mechanics Calculations. A conformational scan on zwitterionic L-prolinium of the dihedral angle *T* has been performed (Scheme 2). We have used density functional theory (DFT) and, more precisely, the PBE0 functional[27−29] and the 6-311G++(d,p) basis set. For this fully relaxed scan, a step size of 10° has been used, so that a total of 36 optimizations have been carried out. Convergence was assumed when the r.m.s. force was smaller than 3 × 10−4 au and the SCF convergence criterion was set to 10−8 au.

Scheme 2. Labelling of Atoms (H Atoms Not Shown) and Dihedral Angles in Prolinium Molecule (*T* Is the Dihedral Angle Defined by N−C4−C5−O1)

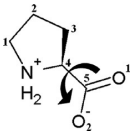

Quantum Mechanics of Crystal Hydrogen-Bonding Stability for Cocrystal L-Pro/Fumaric Acid. In order to qualify relative energies of the new cocrystalline structure formed, comparison between calculated energies of the cocrystal Hydrogen-bonding conformation (between L-proline and fumaric acid) and L-proline and fumaric acid alone using ab initio quantum approximation (GAUSSIAN program[30]) on PBEPBE/6-311++G(d,p) level of theory has been performed. Mulliken set of charges for atoms implicated in the hydrogen bonds are listed in Table 5. Electrostatic potentials for each partner in selected hydrogen bonds are represented in Figure 13.

Rationalization of Intermolecular Interactions by Hirshfeld Surfaces Analysis for Cocrystal L-Pro/Fumaric Acid. Hirshfeld surfaces and molecular fingerprints have been obtained for each coformer in L-pro/fumaric acid zwitterionic cocrystal with Crystal -Explorer v. 3.0.[31]

RESULTS AND DISCUSSION

Preparation of Solid Phases. *L-Prolinium/Fumaric Acid Zwitterionic Cocrystal (2:1 L-Pro$^{\pm}$–Fum).* Powder samples of a 2:1 L-proline (L-Pro) and fumaric acid (Fum) cocrystal were prepared by dry grinding[32] of 1.74 mmol of L-proline and 0.87 mmol of fumaric acid. A few minutes of grinding is sufficient to

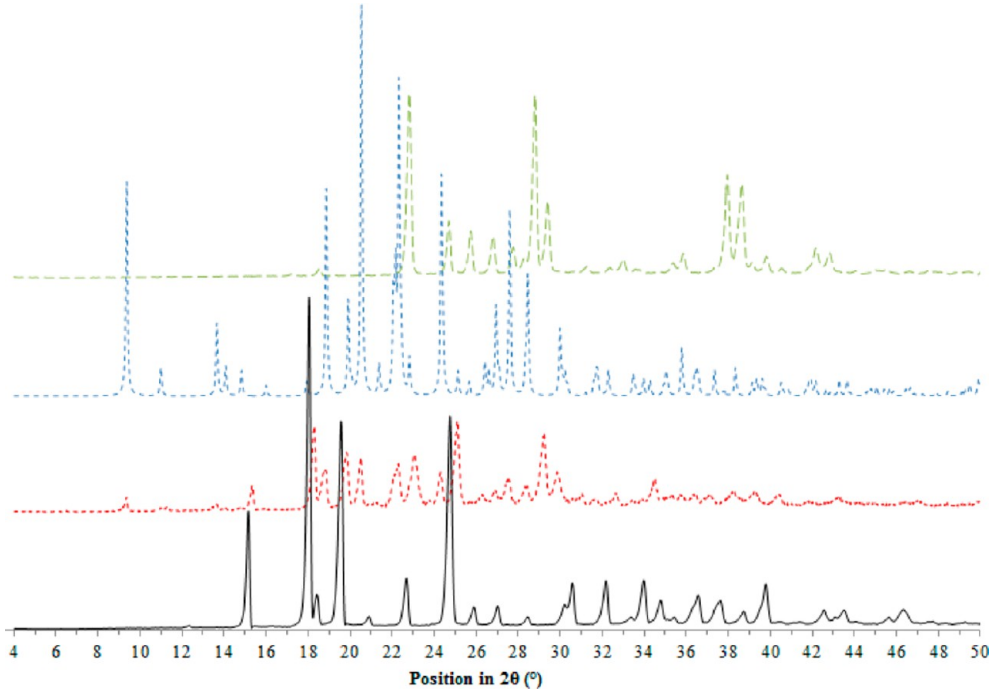

Figure 1. PXRD patterns of L-proline (black), fumaric acid (green dotted), and the 90-min dry-ground sample (red dotted) and the SCXRD powder pattern simulation (blue dotted).

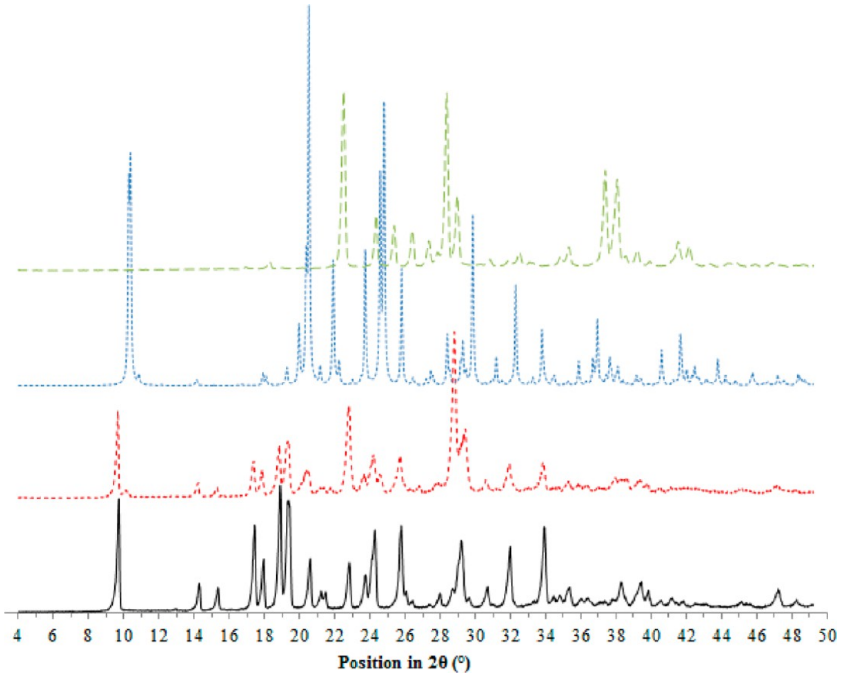

Figure 2. PXRD patterns of DL-proline (black), fumaric acid (green dotted), the 90-min dry-ground sample (red dotted), and the SCXRD powder pattern simulation (blue dotted).

note the appearance of the cocrystal by PXRD. To increase the yield of cocrystal formation, different grinding times were selected and applied,[33] with a maximal amount of cocrystal obtained after 90′ (Figures 1 and S1; by comparison of intensity for peaks at 8.8° and 13.4° in 2θ, which principally characterizes the cocrystal). Longer grinding times (until 720′) produce the same amount of cocrystalline end-product. By following disappearance of the peak at 11.8° in 2θ, representative of L-proline, PXRD confirmed that essentially only the cocrystalline product was formed (through comparison with the simulated powder pattern coming from SCXRD analysis; see section below and Table 1), with small quantities (a few percentages) of crystalline L-proline and fumaric acid remaining (Figures 1 and S1). PXRD is the fastest (and most-employed) method to obtain information about production of cocrystals through grinding, even if this investigation method has its limitations. In fact, if the grinding process potentially produces a small amount of amorphous material, this part will

dx.doi.org/10.1021/cg400081v | *Cryst. Growth Des.* 2013, 13, 2373−2389

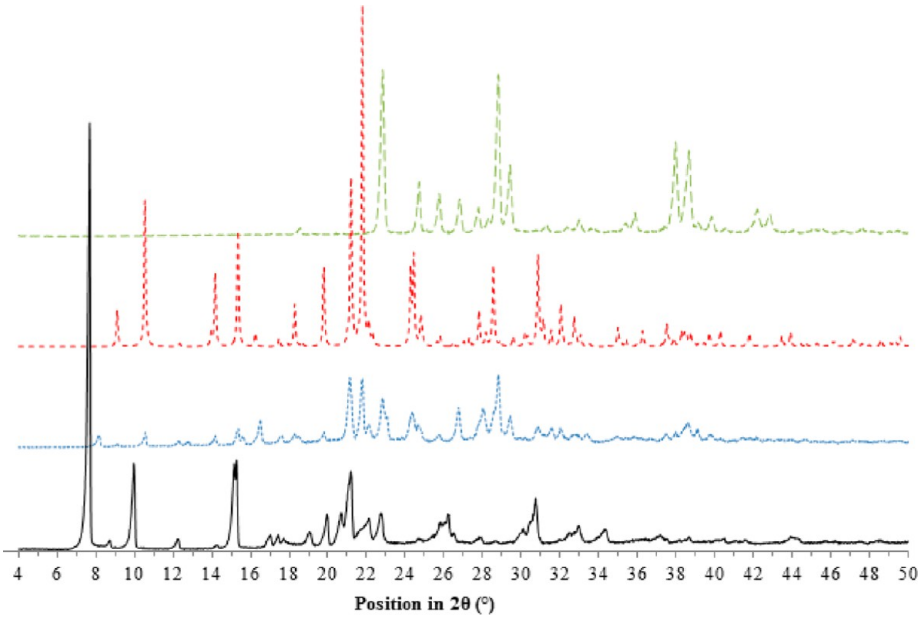

Figure 3. PXRD patterns of D-prolinamide (black), fumaric acid (green dotted), the 90-min dry-ground sample (red dotted), and the SCXRD powder pattern simulation (blue dotted).

Table 1. Crystallographic Data, Data Collection, and Structure Refinement Details

	2:1 L-Pro$^{\pm}$–Fum	2:1 D-Pro$^{\pm}$–Fum	2:1 DL-Pro$^{\pm}$–Fum	2:1 D-ProNH_2^+ –Fum^{2-}
		Crystal Data		
empirical formula	$2(C_5H_9NO_2),C_4H_4O_4$	$2(C_5H_9NO_2),C_4H_4O_4$	$2(C_5H_9NO_2),C_4H_4O_4$	$2(C_5H_{11}N_2O),C_4H_2O_4,\ H_2O$
fw	346.34	346.34	346.34	362.39
crystal syst	monoclinic	monoclinic	orthorhombic	monoclinic
space group	$P2_1$ (No. 4)	$P2_1$ (No. 4)	$Pbc2_1$ (No. 29)	$P2_1$ (No. 4)
a, *b*, *c* (Å)	9.5896(4)	9.5830(1)	17.2025(6)	9.8307(5)
	9.0386(3)	9.0370(1)	9.7993(3)	7.1796(3)
	10.1964(5)	10.1790(1)	27.6106(19)	12.8464(6)
α, β, γ (°)	90, 825.94(7), 90	90, 110.837(9), 90	90, 90, 90	90.00, 99.217(5), 90.00
V (Å^3)	825.94(6)	823.86(16)	4654.4(4)	895.00(7)
Z	2	2	12	2
ρ_{calcd} (g/cm^3)	1.393	1.396	1.483	1.345
Mu (Mo Kα) (/mm)	0.115	0.115	0.122	0.108
F(000)	368	368	2208	388
crystal size (mm)	0.10/0.18/0.35	0.10/0.35/0.50	0.10/0.15/0.40	0.04/0.10/0.20
T (K)	293(2)	293(2)	100(5)	293(2)
		collection data		
radiation (Å)	Mo Kα: 0.71073	Mo Kα: 0.71073	Mo Kα: 0.71073	Mo Kα: 0.71073
θ min and max (°)	3.40–25.00	3.40–25.00	3.20–25.00	3.50–25.00
tot, uniq, *R*(int)	3689, 1560, 0.017	3573, 2540, 0.018	14731, 6452, 0.034	3842, 2803, 0.018
		refinement		
obs data	1367	2119	5359	2572
R [$I > 2\sigma(I)$]	0.0357	0.0492	0.0463	0.0404
wR_2 [all]	0.0931	0.1333	0.1291	0.1030
GOF	0.93	1.05	1.10	1.10
residual density	−0.15, 0.17	−0.18, 0.18	−0.31, 0.58	−0.16, 0.14

become invisible to X-ray diffraction and will affect the cocrystal yield. Other techniques such as Terahertz time-domain spectroscopy allows precise determination of the amount of cocrystal formed by grinding methodology.[34,35] But PXRD has also been employed here, as it is easily accessible to us. Crystallization assays were set up by slow evaporation of 2-propanol saturated solutions of the ground product after dry grinding. Needle-like single crystals of the cocrystal, suitable for X-ray single-crystal diffraction, were obtained after 5 days.

D-Prolinium/Fumaric Acid Zwitterionic Cocrystal (2:1 D-Pro$^{\pm}$–Fum). Powder samples of 2:1 D-proline and fumaric acid cocrystal were prepared by dry grinding of 1.78 mmol of D-proline and 0.89 mmol of fumaric acid. As in the case of L-proline and fumaric acid, a few minutes are sufficient to note appearance of the cocrystal by PXRD. A 90-min grinding produces the 2:1 cocrystal and some residual D-proline and fumaric acid, as assessed by the PXRD patterns of pure constituents and sample after grinding (data not shown).

dx.doi.org/10.1021/cg400081v | *Cryst. Growth Des.* 2013, 13, 2373–2389

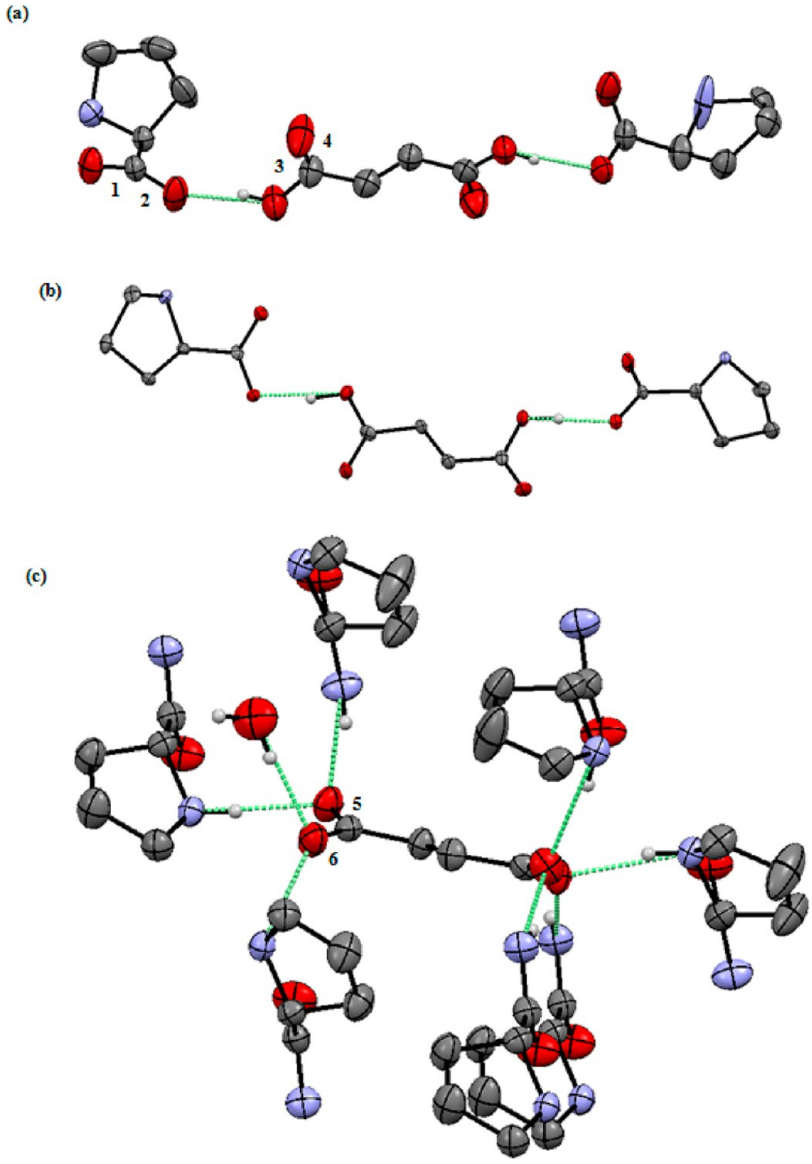

Figure 4. Crystal conformation (ORTEP diagram) drawn with 50% probability ellipsoids of the multicomponent molecular complexes of (a) L-proline/fumaric acid [2:1 L-Pro$^{\pm}$—Fum], (b) DL-proline/fumaric acid [1:1:1 L-Pro$^{\pm}$—Fum—D-Pro$^{\pm}$], and (c) D-prolinamide/fumaric acid [D-ProNH_2^+—Fum$^-$]. The D-proline/fumaric acid [2:1 D-Pro$^{\pm}$—Fum] structure is the mirror image of the structure shown in (a). Hydrogen atoms not involved in hydrogen bonds are omitted for clarity. An alternative conformation of the pyrrolidine ring of proline has been refined but is not represented. Numbers in bold in (a) and (c) are references for C—O bond lengths: **1** = 1.212(4) Å; **2** = 1.302(3) Å; **3** = 1.312(3) Å; **4** = 1.201(4) Å; **5** = 1.260(4) Å; **6** = 1.250(3) Å.

Crystallization assays were set up by slow evaporation of 2-propanol saturated solutions of the ground product after dry grinding. Needle-like single crystals, very similar in size and shape to the 2:1 L-Pro$^{\pm}$—Fum single crystals and suitable for X-ray analysis, were obtained after 5 days.

DL-Prolinium/Fumaric Acid Zwitterionic Cocrystal (1:1:1 L-Pro$^{\pm}$—Fum—D-Pro$^{\pm}$). Powder samples of a DL-proline and fumaric acid cocrystal were prepared by dry grinding of 1.86 mmol of DL-proline and 0.93 mmol of fumaric acid. As in the case of L-proline (or D-proline) and fumaric acid cocrystal, PXRD analysis shows that the cocrystal appears after a few minutes. But after a 90-min grinding time, the conversion seems not to occur as completely as for the other cocrystal grinding experiments, as observed on the Figure 2 comparison with the simulated powder pattern from SCXRD analysis. Nevertheless, several diffraction peaks can be found in common between DL-Pro, the 90-min ground sample and the simulated pattern, making the assignment more difficult. Evaporation of 2-propanol saturated solutions of the ground product after dry grinding leads, after 7 days, to prism-like single crystals suitable for X-ray single-crystal diffraction analysis.

D-Prolinamide/Fumarate Hydrated Salt (2:1 D-ProNH_2^+—Fum^{2-}). Powder samples of a 2:1 D-prolinamide (D-ProNH_2) fumarate salt were prepared by dry grinding of 1.72 mmol of D-prolinamide and 0.87 mmol of fumaric acid. A few minutes grinding is enough to form the salt and 90-min grinding time produced the salt as the major product plus a physical mixture of the starting material, as it can be observed on Figure 3. Moreover, the comparison between powder simulation coming from the single-crystal analysis (see section below, Table 1) shows a really similar pattern. Prism-like single crystals of the salt were obtained, after 5 days, by slow evaporation of 2-

dx.doi.org/10.1021/cg400081v | *Cryst. Growth Des.* 2013, 13, 2373−2389

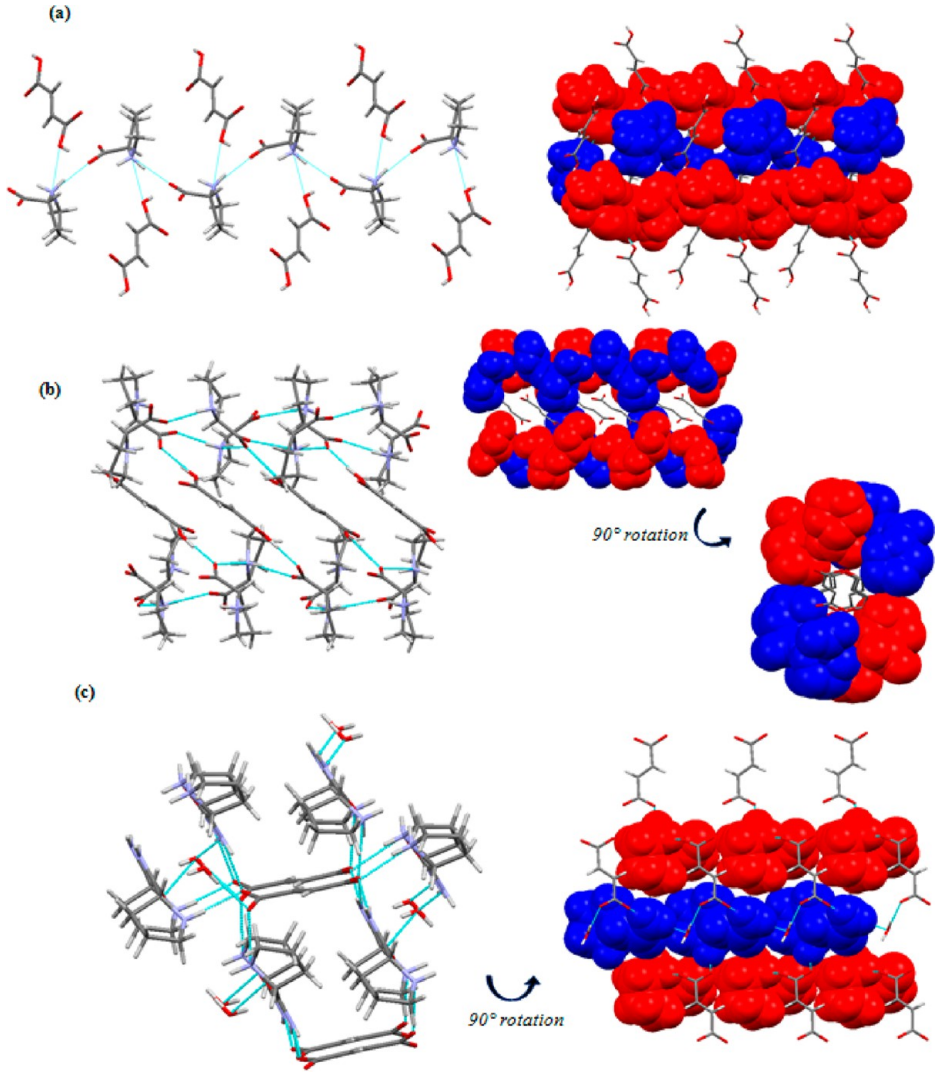

Figure 5. Illustration of the hydrogen bonding network within the single crystal structure of (a) the 2:1 L-Pro$^{\pm}$—Fum cocrystal obtained by grinding L-proline with fumaric acid, (b) DL-proline/fumaric acid [1:1:1 L-Pro$^{\pm}$—Fum—D-Pro$^{\pm}$], and (c) D-prolinamide/fumaric acid [D-ProNH_2^+—Fum$^-$]. Two representations are given for each molecular packing (on the left, the packing organization with hydrogen bonds highlighted and on the right, prolinium (or prolinamide) shown in space-filling models forming infinite columns (red and blue)).

propanol saturated solutions and allowed determination of the crystal structure of the ground product: a 2:1 D-ProNH_2^+—Fum^{2-} salt.

Structure Determination. *L- (and D-) Prolinium/Fumaric Acid Zwitterionic Cocrystal (2:1 L-(D-)Pro$^{\pm}$—Fum).* Single-crystal XRD analysis was performed on needle-like crystals obtained by recrystallization from saturated solutions in 2-propanol of ground samples of L-proline/fumaric acid and D-proline/fumaric acid cocrystals. Main crystallographic data are given in Table 1.

The single-crystal X-ray study reveals that zwitterionic cocrystals, not salts, have been obtained. The structures contain prolinium zwitterions (L- or D-Pro$^{\pm}$) and protonated fumaric acid (Fum) in a 2:1 stoichiometry ratio. Protonation states within the L-prolinium/fumaric acid [2:1 L-Pro$^{\pm}$—Fum] (and D-prolinium/fumaric acid [2:1 D-Pro$^{\pm}$—Fum]) zwitterionic cocrystals (Figure 4a) were unambiguously determined by careful inspection of Fourier difference maps and on the basis of geometries features (C—O bond lengths, Figure 4a,c).

The pK_a difference between the two components in the cocrystals is 1.3 (pK_a for L-Pro: 1.8,[36] pK_a for fumaric acid: 3.1[37]) which means that the formation of these cocrystals is consistent with previous empirical guidelines predicting potential cocrystal formation when $\Delta pK_a < 3.0$.[38] The structures of the zwitterionic cocrystals involving the prolinium entity are also consistent with examples from the literature (CSD refcode: ZEZHIV,[17] IHUMAZ,[18] VESCUS[39]).

Within experimental errors, the conformation of the zwitterionic prolinium, and fumaric acid display no significant differences compared with related structures. However, the zwitterions give rise to different hydrogen-bonded patterns.

In the crystal packing of the 2:1 L-prolinium/fumaric acid cocrystal (and similarly in the enantiomeric structure of the 2:1 D-Pro$^{\pm}$—Fum zwitterionic cocrystal), the zwitterions form columns of infinite double chains, parallel to crystallographic *a*-direction, created by two N—H···O bonds. These columns are cross-linked in the crystallographic *bc*-plane by the diacid fumaric acid molecule as illustrated in Figure 5a (and S2). Table 2 quantifies the contribution of the selected hydrogen bonds to the overall stability of these packings.

These well-organized networks of hydrogen bonds are principally localized around the protonated nitrogen atoms of

dx.doi.org/10.1021/cg400081v | *Cryst. Growth Des.* 2013, 13, 2373−2389

Table 2. Geometrical Parameters (Distance and Angle) of Hydrogen Bonds in the Zwitterionic Cocrystals and Salt Structures Discussed in This Work[40]

H-bonds	D···A distance (Å)	H···A distance (Å)	D−H···A angle (°)	symmetry code
		2:1 L-Pro$^{\pm}$−Fum		
N1--H1C···O4	2.839(14)	2.04	147	$x, 1 + y, z$
N1--H1D···O1	2.538(14)	2.06	112	
N2--H2E···O3	2.807(4)	1.99	150	$2 - x, 1/2 + y, 2 - z$
N2--H2E···O6	3.041(3)	2.47	121	$2 - x, 1/2 + y, 2 - z$
N2--H2F···O3	2.641(4)	2.14	114	
N2--H2F···O1	2.849(4)	2.11	138	$2 - x, -1/2 + y, 2 - z$
N1--H1′3···O2	3.294(14)	2.04	148	$1 - x, 1/2 + y, 2 - z$
O6--H6···O2	2.553(3)	1.74	169	$2 - x, -1/2 + y, 2 - z$
N1--H1′4···O4	2.839(14)	2.25	121	$x, 1 + y, z$
O7--H7E···O4	2.576(4)	1.74(6)	166(6)	$1 - x, -1/2 + y, 1 - z$
		2:1 D-Pro$^{\pm}$−Fum		
N2--H2A···O4	2.644(4)	2.14	115	
N2--H2A···O1	2.850(4)	2.11	138	$1 - x, -1/2 + y, 2 - z$
N2--H2B···O4	2.798(4)	1.98	151	$1 - x, -1/2 + y, 2 - z$
N2--H2B···O5	3.035(3)	2.47	121	$1 - x, -1/2 + y, 2 - z$
N1′--H1′1···O1	2.579(8)	2.13	110	
N1′--H1′2···O3	2.751(7)	1.93	151	
O5--H5F···O2	2.561(4)	1.75	170	$1 - x, -1/2 + y, 2 - z$
O7--H7F···O3	2.578(4)	1.78	164	$-x, 1/2 + y, 1 - z$
N4--H4E···O2	2.719(3)	2.32(3)	108(2)	
N4--H4E···O3	2.766(3)	1.99(3)	148(2)	
O7--H7D···O3	2.791(3)	1.95(5)	170(8)	$1 - x, 1/2 + y, 1 - z$
O7--H7E···O2	2.924(3)	2.21(8)	146(7)	$x, 1 + y, 1 + z$
		2:1 DL-Pro$^{\pm}$−Fum		
N01--H01B···O01	2.677(4)	2.18	110	
N01--H01B···O02	3.025(4)	2.21	141	$1 - x, 1/2 + y, z$
N01--H01A···O91	2.749(5)	1.91	156	$1 - x, 1/2 + y, z$
O102--H102···O62	2.553(4)	1.57	168	
N51--H51A···O51	2.672(5)	2.16	113	
N51--H51B···O61	2.744(5)	1.86	154	$-x, 1/2 + y, z$
N51--H51B···O102	3.101(4)	2.59	114	$-x, 1/2 + y, z$
N61--H61B···O61	2.683(5)	2.21	113	
N71--H71B···O71	2.680(5)	2.27	106	
N71--H71B···O72	2.867(4)	2.01	156	$-x, 1/2 + y, z$
N81--H81B···O81	2.679(4)	2.22	110	
N91--H91B···O91	2.689(4)	2.22	108	
O204--H204···O92	2.558(4)	1.59	174	
O304--H304···O72	3.240(5)	2.55	143	$-x, 1/2 + y, z$
		2:1 D-ProNH_2^+−Fum^{2-}		
N1--H1D···O6	2.746(3)	1.89(3)	167(3)	$-x, 1/2 + y, 1 - z$
N1--H1E···O1	2.685(3)	2.32(3)	103(2)	
N1--H1E···O5	2.902(3)	2.02(3)	160(2)	
N2--H2D···O7	3.009(4)	2.17(4)	164(4)	$x, -1 + y, z$
N2--H2E···O4	2.901(3)	2.04(3)	166(3)	$1 - x, 1/2 + y, 1 - z$
N3--H3D···O6	2.860(3)	2.01(4)	168(4)	$-x, 1/2 + y, -z$
N3--H3E···O5	2.929(3)	2.09(4)	164(3)	$-x, -1/2 + y, -z$
N4--H4D···O4	2.780(3)	1.89(3)	175(2)	$1 - x, 1/2 + y, -z$
N4--H4E···O2	2.719(3)	2.32(3)	108(2)	
N4--H4E···O3	2.766(3)	1.99(3)	148(2)	
O7--H7D···O3	2.791(3)	1.95(5)	170(8)	$1 - x, 1/2 + y, 1 - z$
O7--H7E···O2	2.924(3)	2.21(8)	146(7)	$x, 1 + y, 1 + z$

proline and involve the oxygen atoms of the prolinium carboxylate and the fumaric acid, leading to a fairly dense organization of the crystalline structures. In both structures, hydrogen-bonded single chains of proline molecules are organizing the structures, and, inserted between them, fumaric acid molecules play the role of hydrogen-bonding linkers between chains with the same orientation. Those hydrogen bonds (Table 2) can be classified as moderate[40] and play a major influence on the crystal packing.

First-level graph sets for the proline aggregates in the 2:1 L-(or D-)-Pro$^{\pm}$−Fum zwitterionic cocrystal are of two types: finite groups $D^1_1(2)$ or infinite chains $C^1_1(5)$ (Figures 6a and S3A).

dx.doi.org/10.1021/cg400081v | Cryst. Growth Des. 2013, 13, 2373−2389

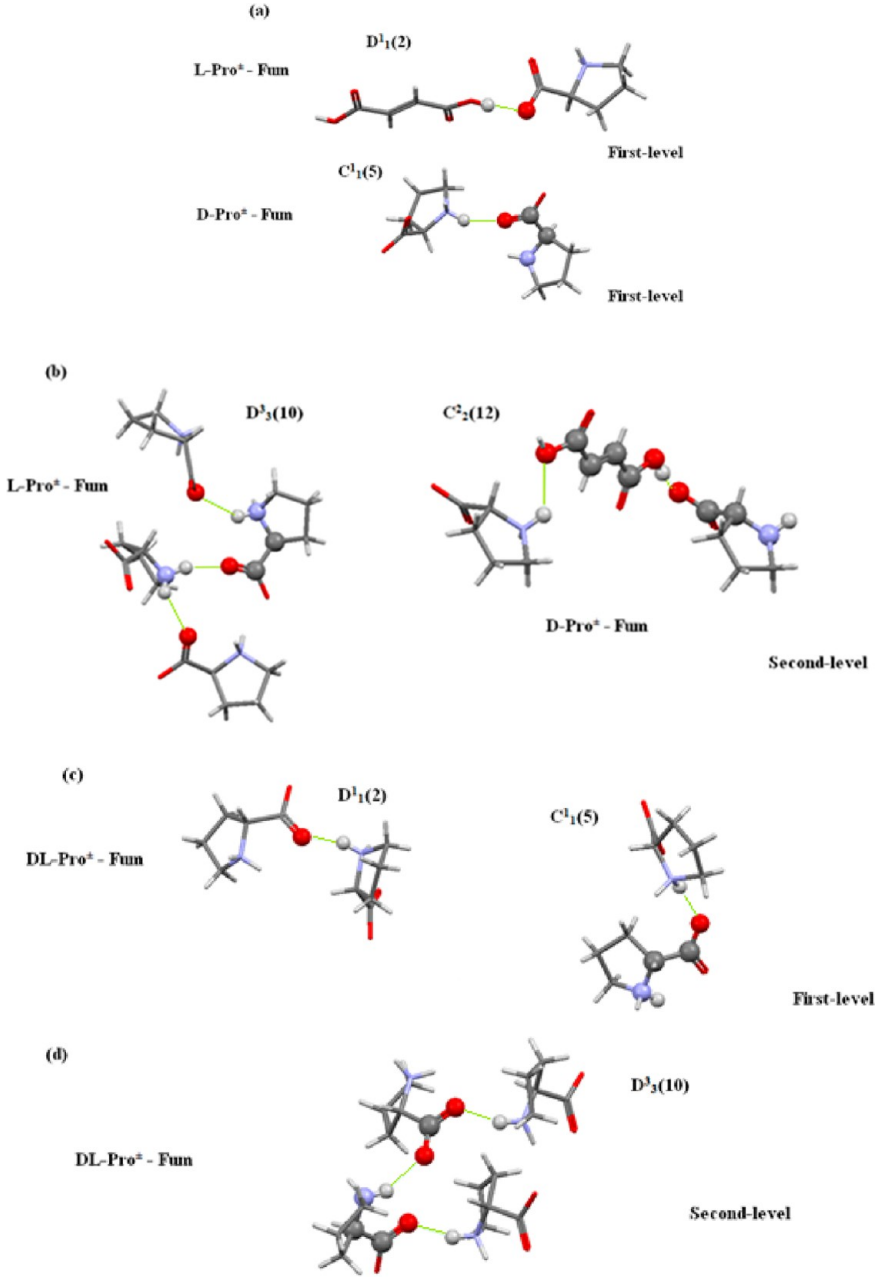

Figure 6. (a–d) Selected first- and second-level graph-set patterns for zwitterionic cocrystals/salt from the work.

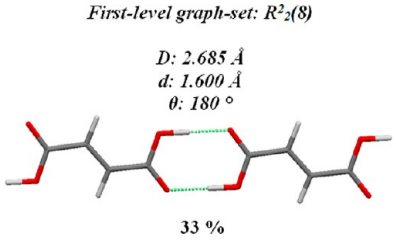

Figure 7. Geometrical parameters of carboxylic acid homosynthon strong hydrogen bond (D = D···A distance; d = H···A distance; θ = D–H···A angle) for fumaric acid and its occurrence stability in the Cambridge Structural Database.[41,45]

This demonstrates similarities with the major first-level graph-set patterns of other structures implying prolinium in Cambridge Structural database[41] (CSD), like in entries ZEZHIV[17] or VESCUS[39] (Figure S3A).

Second-level graph sets for the proline aggregates in the 2:1 L- (or D-)-Pro±–Fum zwitterionic cocrystal are of two types: finite groups D (until 10 elements) or infinite chains C (until 12 elements) (Figures 6b and S3B). This demonstrates similarities with the major second-level graph-set patterns of other structures implying prolinium in CSD,[38] like in VESCUS[39] (Figure S3B).

The large number of potential hydrogen-bond donors (eight for the asymmetric unit) and acceptors (eight for the asymmetric unit) justifies the presence of a complex network of hydrogen bonds in the crystal packing. Among the hydrogen bond sites, one zwitterion of L(D)-prolinium is the most implicated: six different hydrogen bonds are related to this entity, with four hydrogen bonds with another L(D)-prolinium molecule and two hydrogen bonds with fumaric acid. As a

dx.doi.org/10.1021/cg400081v | Cryst. Growth Des. 2013, 13, 2373–2389

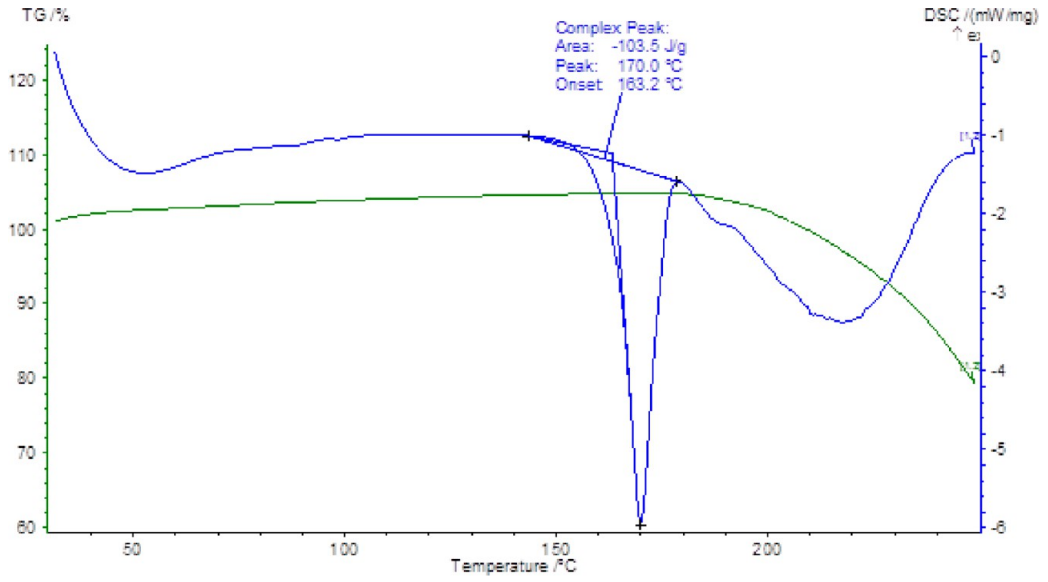

Figure 8. DSC thermogram (and TGA monitoring, showing the compound degradation by sublimation after the melting point) of the zwitterionic cocrystal L-Pro$^{\pm}$—Fum (measured melting point (onset temperature): 163.2 °C (20 K/min)).

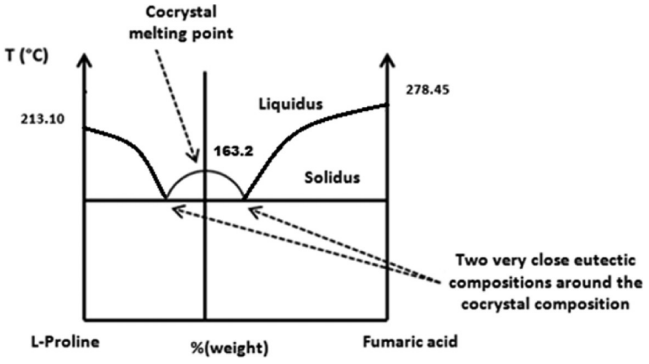

Figure 9. Schematized binary phase diagram for cocrystal 2:1 L-Pro$^{\pm}$—Fum (eutectic compositions are represented symmetrically here, but they are not necessarily symmetrical around the cocrystal composition).

result, the average density for L(D)-prolinium zwittericonic cocrystal is relatively high with calculated density ranging from 1.363 to 1.369 g/cm^3.

Fumaric acid is known to exist under at least two polymorphic arrangements (monoclinic: FUMAAC[42] and FUMAAC02[43] and anorthic: FUMAAC01[44] and FUMAAC03[45]), in both of which molecules form chains connected by hydrogen bonds involving the two carboxylic acid extremities in a classical dimeric arrangement. In the cocrystals, those hydrogen bonds between fumaric acids are replaced by hydrogen bonds between the carboxylic acids of fumaric acid and the carboxylate moieties of prolinium (but there is also a hydrogen bond with the cyclic amine moiety of prolinium), confirming the ability of Pro$^{\pm}$ to disrupt the classical dimeric homosynthon arrangement involving the carboxylic acid groups (Figure 7; see Point 3.6).

The calculated morphology (Figure S4), determined with the BFDH method, corresponds to the crystal habit of the 2:1 L-prolinium/fumaric acid cocrystal.

DL-Prolinium/Fumaric Acid Zwitterionic Cocrystal (1:1:1 L-Pro$^{\pm}$—Fum—D-Pro$^{\pm}$). SCXRD analysis was also performed on the single crystals obtained by recrystallization from saturated solutions in 2-propanol of ground samples of racemic DL-proline and fumaric acid. Main crystallographic data are given in Table 1, and Figure 4b presents the conformation of the molecules in the complex. The molecules in the crystal have standard geometry parameters and are consistent with a zwitterionic form of both D- and L-prolinium and a protonated fumaric acid, leading to the DL-prolinium/fumaric acid zwitterionic cocrystal (1:1:1 L-Pro$^{\pm}$—Fum—D-Pro$^{\pm}$). Here again, molecular packing is determined by formation of intermolecular hydrogen bonds (Figure 5b, Table 2).

From a structural point of view, an organization similar to one of the zwitterionic cocrystals involving L-proline or D-proline and fumaric acid is observed: hydrogen-bonded double chains of prolinium zwitterions organize the network with fumaric acid molecules inserted between them. But in the case of the ground samples of racemic DL-proline and fumaric acid, channel-like cavities are formed by fumaric acid molecules cross-linking the chains through hydrogen bonds.

First-level graph sets for the proline aggregates in the 2:1 DL-Pro$^{\pm}$—Fum zwitterionic cocrystal are of two types: finite groups $D^1_1(2)$ or infinite chains $C^1_1(5)$ (Figure 4c). This arrangement is similar to the one observed for L- (or D-)-Pro$^{\pm}$—Fum zwitterionic cocrystal and also demonstrates similarities with the major first-level graph-set patterns of other structures implying prolinium in CSD (LABZUJ[46]) (Figures 6c and S3C).

Second-level graph sets for the proline aggregates in the 2:1 L DL-Pro$^{\pm}$—Fum zwitterionic cocrystal are of finite groups D (until 10 elements) (Figure 4d). This demonstrates similarities with the major second-level graph-set patterns of other structures implying prolinium in CSD,[41] like in entry VESCUS[39] (Figure S3B).

The large number of potential hydrogen bond donors (18 for the asymmetric unit) and acceptors (18 for the asymmetric unit) also justifies — like in the case of L(D)-Pro$^{\pm}$—Fum zwitterionic cocrystal — the presence of a dense network of hydrogen bonds in the crystal packing. Among the hydrogen bond sites, prolinium ions are the most implicated (like L(D)-Pro$^{\pm}$—Fum): five different hydrogen bonds are related to prolinium, with four hydrogen bonds with other prolinium ions and one hydrogen bond with fumaric acid. But in this case,

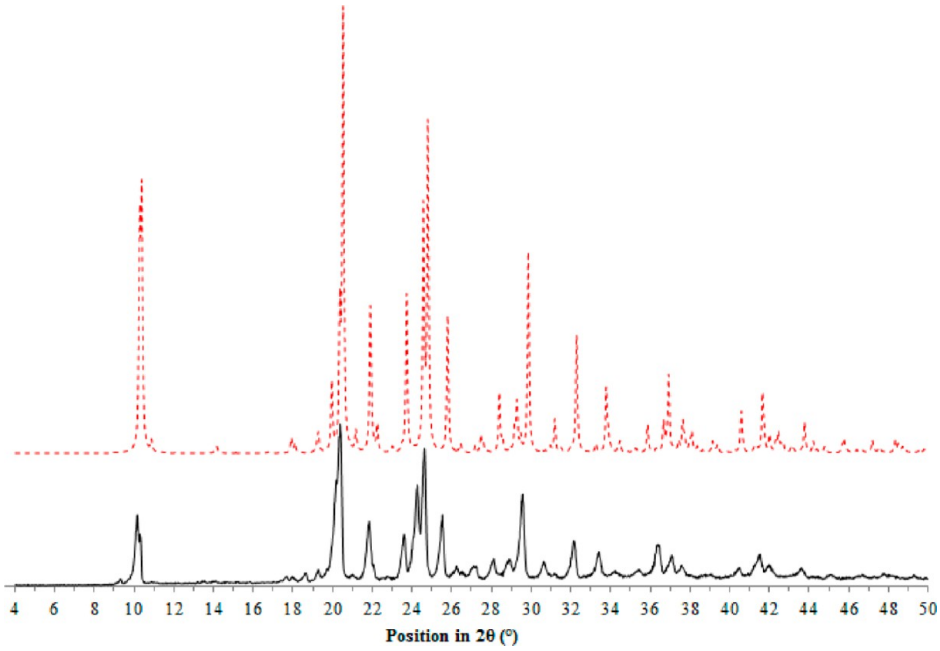

Figure 10. PXRD patterns comparison of DL-proline/fumaric acid zwitterionic cocrystal (black), produced by grinding of the two chiral cocrystals, L-proline/fumaric acid fumaric acid and D-proline/fumaric acid, and of the simulated powder pattern from SCXRD analysis (red dotted).

Scheme 3. Overall View of All the Structures Implying Prolinium Formed and Highlighting of Two Modes of Cocrystal Reactivity

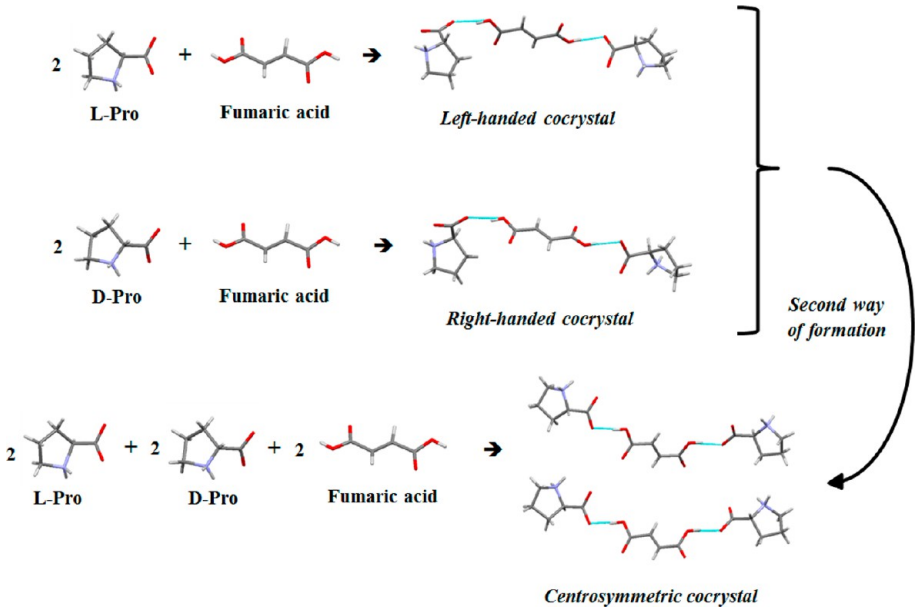

even with an average reduced hydrogen bonding interaction compared to L(D)-Pro$^{\pm}$–Fum, the calculated density for DL-prolinium zwitterionic cocrystal is higher: 1.483 g/cm^3. This result demonstrates that the hydrogen bonding interaction network is not solely the driving force to a dense crystalline network: other effects like geometric fit and sterical hindrance should also be taken into account.[47−49]

D-Prolinamide/Fumarate Hydrated Salt (2:1 D-ProNH$_2^+$–Fum^{2-}). Prolinamide has been selected because, in contrast to proline, it cannot exist under zwitterionic form, and we were curious about the possible formation of a new multimolecular complex and its structural organization. The crystal structure of single crystals obtained by recrystallizing ground samples of D-prolinamide and fumaric acid from saturated solutions in 2-propanol confirms that a salt is formed between one dideprotonated fumarate ion (Fum^{2-}) and two protonated D-prolinamide molecules (D-ProNH$_2^+$) (Figure 4c). Geometry parameters (e.g., C−O bond lengths, Figure 4) are consistent with a salt structure (2:1 D-ProNH$_2^+$–Fum^{2-}) and clearly distinct from the structures of the prolinium-fumaric acid zwitterionic cocrystals. A water molecule further cocrystallizes in this system, leading to a hydrated salt. As it can be seen in Figure 4, the powder pattern of the ground sample is almost identical to the SCXRD simulation pattern (excepted for traces coming from the physical mixture of the two precursors), leading to the conclusion that even if no water was intentionally

Table 3. Main Characteristics and Differences between Structures from CSD and Cocrystals Discussed Here

structure name (CSD refcode)	formula	space group	lattice parameters (Å)	lattice parameters (deg)	cell volume	Z	R (%)
cocrystal from the work	$2(C_5H_9NO_2),C_4H_4O_4$	$P2_1$	*a* 9.589(4)	*α* 90.00	825.94(2)	2	3.69
			b 9.038(3)	*β* 110.84(5)			
			c 10.196(5)	*γ* 90.00			
cocrystal from the work	$2(C_5H_9NO_2),C_4H_4O_4$	$P2_1$	*a* 9.5830(10)	*α* 90.00	823.86(16)	2	4.74
			b 9.0370(10)	*β* 110.837(9)			
			c 10.1790(10)	*γ* 90.00			
cocrystal from the work	$2(C_5H_9NO_2),C_4H_4O_4$	$Pca2_1$	*a* 17.2025(6)	*α* 90.00	4654.4(4)	12	5.33
			b 9.7993(3)	*β* 90.00			
			c 27.6106(19)	*γ* 90.00			
hydrated salt from the work	$2(C_5H_{11}N_2O),C_4H_2O_4,H_2O$	$P2_1$	*a* 9.8307(5)	*α* 90.00	895.00(7)	2	4.04
			b 7.1796(3)	*β* 99.217(5) *γ*			
			c 12.8464(6)	90.00			
LABZUJ[46]	$C_5H_9NO_2,0.5(C_4H_6O_4)$	$P2_1/c$	*a* 5.254(1)	*α* 90.00	816.9(1)	4	4.50
			b 17.480(1)	*β* 119.60(6)			
			c 10.230(1)	*γ* 90.00			
CADKOJ[62]	$C_5H_{10}NO_2^+,C_5H9NO_2,BF_4^-$	$P2_1$	*a* 7.7860(5)	*α* 90.00	726.75(8)	2	7.17
			b 7.3654(4)	*β* 90.088(1)			
			c 12.6730(9)	*γ* 90.00			
CADKUP[62]	$C_5H_{10}NO_2^+,C_5H_9NO_2,Br^-$	$P4_12_12$	*a* 12.8482(6)	*α* 90.00	2709.3(3)	8	3.57
			b 12.8482(6)	*β* 90.00			
			c 16.4126(7)	*γ* 90.00			
CADLIE[62]	$C_5H_{10}NO_2^+,C_5H_9NO_2,Cl^-$	$P4_12_12$	a 12.8188(4) b	*α* 90.00	2643.5(4)	8	5.20
			12.8188(4) c	*β* 90.00			
			16.0876(7)	*γ* 90.00			
CIDBOH[56]	$2(C_5H_9\ NO_2),C_7H_7NO_2,H_2O$	$P2_1$	*a* 9.8171(6)	*α* 90.00	963.86(5)	2	4.40
			b 10.416(11)	*β* 112.078(9)			
			c 10.171(12)	*γ* 90.00			
DUKJUP[55]	$C_5H_9NO_2,C_{29}H_{28}F_6N_4OS,CH_4O$	$P2_12_12_1$	*a* 11.597(3)	*α* 90.00	3616.4(4)	4	6.0
			b 13.044(4)	*β* 90.00			
			c 23.907(7)	*γ* 90.00			
GIVROS[63]	$C_5H_9NO_2,C_{18}H_{14}O_4$	$P2_12_12_1$	*a* 8.436(8)	*α* 90.00	2033.3(2)	4	5.07
			b 18.988(12)	*β* 90.00			
			c 12.6937(11)	*γ* 90.00			
IDINAK[64]	$C_5H_{10}NO_2^+,C_5H_9NO_2,ClO_4^-$	$P2_1$	*a* 7.848(6)	*α* 90.00	744.74(1)	2	5.10
			b 7.3951(14)	*β* 90.95(4)			
			c 12.834(5)	*γ* 90.00			
IHUMAZ[18]	$C_5H_9NO_2,C_{10}H_6N_2O$	$P2_1$	*a* 14.755(17)	*α* 90.00	1368.0(5)	4	5.29
			b 5.2827(6)	*β* 111.44(2)			
			c 18.856(2)	*γ* 90.00			
KECJIM[65]	$C_5H_9NO_2,C_8H_{11}BO_3$	$P1$	*a* 7.3764(6)	*α* 84.112(7) *β*	704.32(7)	2	5.25
			b 7.8303(7)	78.719(7) *γ*			
			c 12.9586(10)	73.907(7)			
LUDFOF[66]	$C_5H_{10}NO_2^+,\ C_5H_9NO_2,NO_3^-$	$P2_12_12_1$	*a* 7.2006(6)	*α* 90.00	1335.9(1)	4	4.69
			b 7.711(1)	*β* 90.00			
			c 24.060(3)	*γ* 90.00			
OLIZAL[19]	$2(C_5H_{10}NO_2^+),\ 2(C_5H_9NO_2),2(C_{12}H_4N_4^-),\ C_{12}H_4N_4$	$P2_12_12$	*a* 34.868(3)	*α* 90.00	2597.7(3)	2	4.53
			b 7.7456(6)	*β* 90.00			
			c 9.6186(7)	*γ* 90.00			
POKHAY10[67]	$C_5H_9NO_2,C_{23}H_{28}O_3$	$P2_1$	*a* 11.650(3)	*α* 90.00	2643.4(9)	4	5.30
			b 8.530(7)	*β* 97.60(1)			
			c 26.837(3)	*γ* 90.00			
VESCUS[40]	$C_5H_9NO_2,C_{12}H_{12}O_4$	$P2_1$	*a* 7.745(2)	*α* 90.00	781.00(4)	2	2.51
			b 8.028(3)	*β* 90.00			
			c 12.561(4)	*γ* 90.00			
ZEZHIV[17]	$C_5H_9NO_2,C_7H_6O_4$	$P2_12_12_1$	*a* 5.896(2)	*α* 90.00	1220.7(1)	4	3.9
			b 11.486(1)	*β* 90.00			
			c 18.016(3)	*γ* 90.00			
PROLIN[52]	$C_5H_9NO_2$	$P2_12_12_1$	*a* 11.55	*α* 90.00	541.74(1)	4	16.9

dx.doi.org/10.1021/cg400081v | *Cryst. Growth Des.* 2013, 13, 2373−2389

Table 3. continued

structure name (CSD refcode)	formula	space group	lattice parameters (Å)	lattice parameters (deg)	cell volume	Z	R (%)
			b 9.02	*β* 90.00			
			c 5.2	*γ* 90.00			
QANRUT[53]	$C_5H_9NO_2$	$P2_1/c$	*a* 8.9906(6)	*α* 90.00	542.699	4	3.95
			b 5.2987(4)	*β* 97.041(2)			
			c 11.4786(8)	*γ* 90.00			

Table 4. Main Characteristics and Differences between Structures from CSD and Cocrystals Discussed Here (Composition of Cocrystals from Table 3)

structure name (CSD refcode)	composition
cocrystal from the work	L-prolinium and fumaric acid
cocrystal from the work	D-prolinium and fumaric acid
cocrystal from the work	DL-prolinium and fumaric acid
hydrated salt from the work	D-prolinamide and fumarate
LABZUJ[46]	DL-prolinium and hemisuccinic acid
CADKOJ[62]	L-prolinium and L-proline tetrafluoroborate
CADKUP[62]	L-prolinium and L-proline bromide
CADLIE[62]	L-prolinium and L-proline chloride
CIDBOH[56]	L-prolinium monohydrate and 4-aminobenzoic acid
DUKJUP[55]	L-prolinium methanolate and (*S*,*R*,*R*,*R*,*S*,*S*)-1-[3,5-bis(trifluoromethyl)phenyl]-3-[(5-ethenyl-1-azabicyclo[2.2.2]octan-2-yl)(6-methoxyquinolin-4-yl) methyl] thiourea
GIVROS[63]	L-prolinium and (11*R*,12*R*)-(+)-9,10-dihydro-9,10-ethanoanthracene-11,12-dicarboxylic acid
IDINAK[64]	L-prolinium and L-proline perchlorate
IHUMAZ[18]	L-prolinium and 1,1-dicyano-2-(4-hydroxyphenyl)ethene
KECJIM[65]	L-prolinium 4-ethoxyphenylboronic acid
LUDFOF[66]	L-prolinium and L-proline nitrate
OLIZAL[19]	L-prolinium and bis(2-carboxypyrrolidinium) bis(7,7,8,8-tetracyanoquinodimethanide) bis(tetracyanoquinodimethane)
POKHAY10[67]	L-prolinium and 4-(2,4,6-tri-isopropyl-benzoyl) benzoic acid
VESCUS[40]	L-prolinium and pentacyclodecane-2,5-dicarboxylic acid
ZEZHIV[17]	L-prolinium and 2,5-dihydroxybenzoic acid
PROLIN[52]	L-prolinium
QANRUT[53]	DL-prolinium

engaged in the grinding process, adsorption from the air during the preparation of the sample may have occurred, finally forming a hydrated salt.

The newly formed structure presents similarities with the zwitterionic cocrystal implying L(D)-proline and fumaric acid, as hydrogen-bonded prolinamide chains are linked between them by fumarate ions sterically inserted among chains, with in this case water molecules that play a part as a hydrogen-bonding mediator between prolinamide and fumarate ions. Molecular packing (Figure 5c) is thus largely stabilized by a dense network of hydrogen bonds (Table 2) that also involves a cocrystallized water molecule, positively charged prolinamide molecules, and the fully deprotonated fumarate ions. First-level graph sets for the prolinamide aggregates in the 2:1 D-ProNH_2^+−Fum salt are of two types: finite groups $D^1_1(2)$ or infinite chains $C^1_1(5)$ (Figure S3D). This arrangement is similar to that of L- (or D)-Pro$^{\pm}$−Fum zwitterionic cocrystal but cannot be compared to existing structures because of the absence of crystalline structures implying prolinamide in CSD. Second-level graph sets for the prolinamide aggregates are also of two types: finite groups D (until 8 elements) or infinite chains C (until 12 elements) (Figure S3E).

The large number of potential hydrogen bond donors (10 for the asymmetric unit) and acceptors (6 for the asymmetric unit) justifies the presence of a dense and complex network of hydrogen bonds in the crystal packing. Among the hydrogen bond sites, fumaric acid is the most implicated: eight different hydrogen bonds are related to this molecule, with seven hydrogen bonds with D-prolinamide molecules and only one hydrogen bond with a water molecule. As a result, the average density for a 2:1 D-ProNH_2^+−Fum salt is relatively high with a calculated density of 1.345 g/cm^3.

Thermal Analysis for L-Proline/Fumaric Acid Zwitterionic Cocrystal. Melting point of the 2:1 L-Pro$^{\pm}$−Fum zwitterionic cocrystal has been measured using DSC and compared to the melting points of the starting coformers, L-proline and fumaric acid (Figure 8). The cocrystal melts at 163.2 °C (onset temperature), whereas the melting point values for L-proline and fumaric acid are 213.1 and 278.4 °C (data not shown) respectively. On one hand, decomposition for L-proline always occurs after the melting point. On the other hand, fumaric acid presents a solid−solid transformation between two monoclinic forms at 205−210 °C and begins to sublime above 210 °C.[49] With these first data, the cocrystal system melting phase diagram is expected to present two eutectic compositions (very close to the cocrystal composition), a classical situation for a cocrystal system, and is schematized in Figure 9. For further DSC analysis (in order to obtain the experimental binary melting diagram), conditions will have to be adapted to take into account degradation and sublimation of the two precursors of the cocrystal.

Synthesis of 2:1 DL-Proline/Fumaric Acid Zwitterionic Cocrystal: Two Synthetic Routes. DL-Proline and fumaric acid grinding, even if it produces partial conversion (Figure 3), has provided the formation of a centrosymmetric three-component zwitterionic cocrystal including the racemic proline and fumaric acid, in a 1:1:1 stoichiometric ratio: 1:1:1 L-Pro$^{\pm}$−Fum−D-Pro$^{\pm}$.

Interestingly, this structure can also be found by direct grinding of the two chiral zwitterionic cocrystals L-proline/fumaric acid [2:1 L-Pro$^{\pm}$−Fum] and D-proline/fumaric acid [2:1 D-Pro$^{\pm}$−Fum]. The resulting ground product shows a PXRD pattern which presents a lot of similarities with the grinding result of DL-proline and fumaric acid (Figure 10), indicating that the same multicomponent structure is produced (Scheme 3). Single-crystals were grown in the same conditions as for the grinding of DL-proline and fumaric acid and analyzed by SCXRD; cell parameters of the 1:1:1 L-Pro$^{\pm}$−Fum−D-Pro$^{\pm}$ cocrystal have been obtained. Similar cocrystal-cocrystal reactions are rare but have been described for two different molecules by other groups.[50,51]

dx.doi.org/10.1021/cg400081v | *Cryst. Growth Des.* 2013, 13, 2373−2389

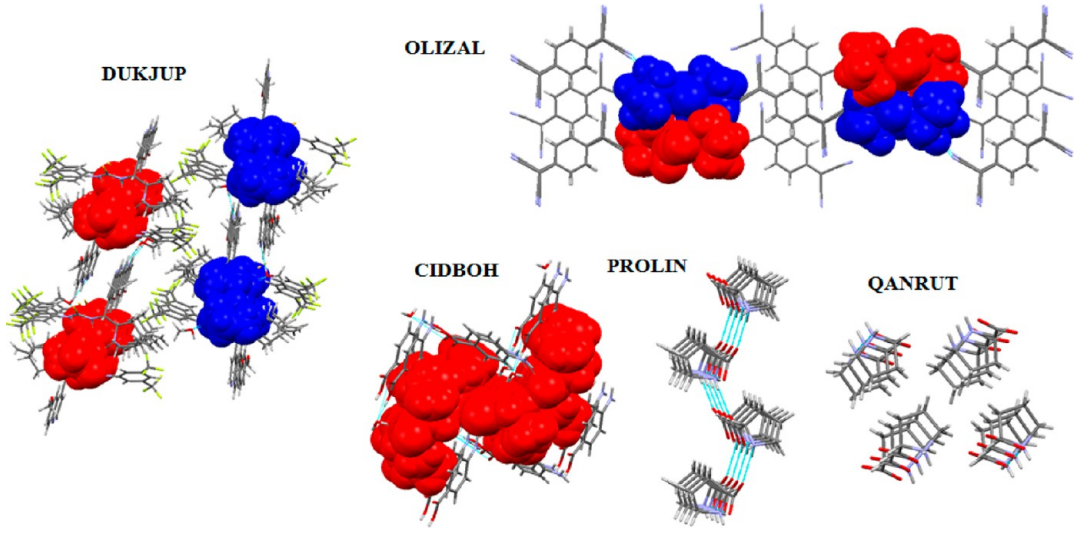

Figure 11. Selection of hydrogen bonding network and molecular packing among cocrystal structures involving the prolinium (L- or DL-prolinium itself) building block retrieved from CSD.

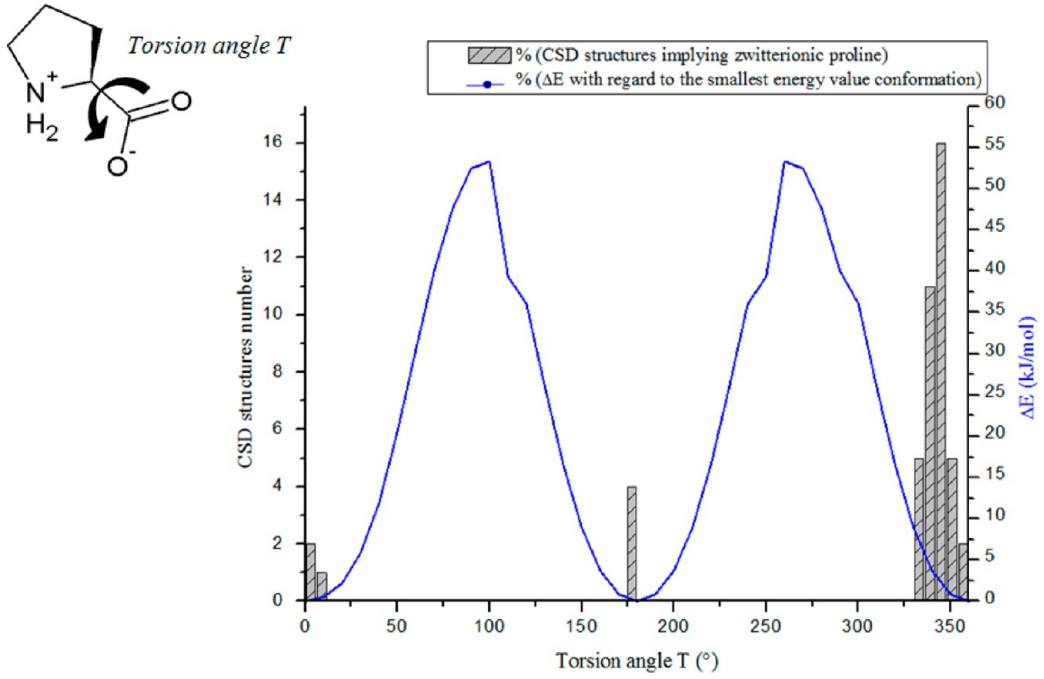

Figure 12. Comparison between evolution of relative energies for each conformation in L-prolinium in regard to the torsion angle *T* (results from conformational scan) and repartition histogram (in function of *T* angle) of structures implying prolinium in CSD. All structures are located in minima conformational regions.

Structural Comparison with Existing Structures in CSD Implying Zwitterionic Pro. The probability of forming a zwitterion cocrystal involving proline rather than a salt can be estimated by examining the Cambridge Structural Database:[41] the majority of structures are in favor of salt formation (136 structures of organic or metallic salts) as opposed to cocrystals (15 organic zwitterionic cocrystal structures). A similar tendency had already been observed by Timofeeva et al.[18] Focusing our search in the CSD on cocrystals structures involving zwitterionic proline, the 15 structures that are found are listed in Tables 3 and 4. Crystal structures of Pro alone (L-Pro: PROLIN[52] and DL-Pro: QANRUT[53]) are also included for comparison.

These structures present similarities with the cocrystal structures discussed here.[52] In particular, cell parameters along the molecular chains for a majority of the structures are close to 5.2 Å (or a dubbled value), broadening a similar previous observation on a smaller subset of structures.[18] In the case of L-prolinium or DL-prolinium alone, 5.2 Å is the value of the parameter along the molecular chain axis. But some exceptions exist, principally for structures implying proline and prolinium in the same unit cell. These structures are different from a classical scheme for a zwitterionic cocrystal, and the cell parameters do not obey to this rule guided by the packing of proline alone. In the opposite of this geometrical finding, the organization of the packing for these structures follows the same organization as that of all the others structures. Molecular

dx.doi.org/10.1021/cg400081v | *Cryst. Growth Des.* 2013, 13, 2373−2389

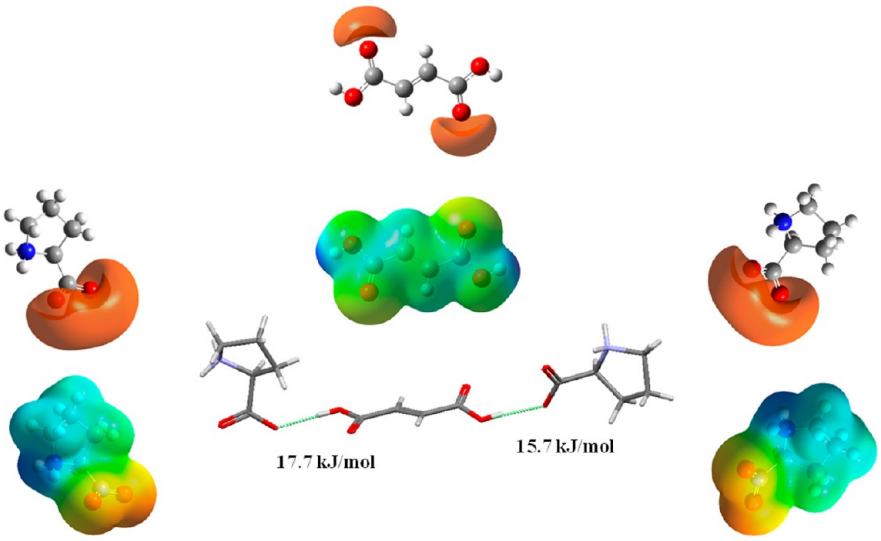

Figure 13. H-bonds heterosynthon between L-prolinium and fumaric acid considered for theoretical relative energy determination of the two H-bonds implicated in the multimolecular fragment (negative attractive potentials and global electrostatic potential (mapped on density surface) at 0.04 $e^-/Å^3$ are also represented).

Table 5. Mulliken Charges of Implicated Atoms in Hydrogen Bonds (Figure 13)

hydrogen bonds	previous Mulliken partial charge value for oxygen (fumaric acid)	new Mulliken partial charge value for oxygen (fumaric acid)	previous Mulliken partial charge value for oxygen (proline)	new Mulliken partial charge value for oxygen (proline)
hydrogen bond A (17.7 kJ/mol)	−0.115	−0.167	−0.385	−0.378
hydrogen bond B (15.7 kJ/mol)	−0.115	−0.205	−0.385	−0.372

packing can best be described by chains of $Pro^{\pm}$ building blocks, linked or not by N−H···O H-bonds between prolinium moieties. Depending principally on the geometry of the partner molecule in the cocrystal, the number of cross-linking chains can vary between one (DUKJUP[55]) to four (OLIZAL[17]), forming real columns in the structure. However, the chains can also be assembled to form infinite sheets of proline entities in the crystal (CIDBOH[56]). In structures implying L-Pro or DL-Pro, the same organization between molecules exists: the two structures are organized in columns, linked by hydrogen bonds between the molecules and, in the case of PROLIN,[52] linked by hydrogen bonds between the different columns too. Selected examples of representative arrangements are shown in Figure 11 (and Figures S5A−D) and are to be compared to the molecular packing reported in the present work (Figure 5). In the case of L(D)-proline/fumaric acid zwitterionic cocrystal, the structure is composed of sheets of prolinium moieties, linked by N−H···O H-bonds and in which molecules of the coformer (fumaric acid) are inserted, and further linked by hydrogen bonds to prolinium. But DL-proline/fumaric acid zwitterionic cocrystal and prolinamide salt are more column-organized, with channel-like cavities in which the fumaric acid can be placed, and linked by hydrogen bonds to the organizing supramolecular synthons that are the prolinium columns. A principal difference exists in structures from CSD: the link between all the columns in the crystalline structures. For some of the structures (DUKJUP,[55] IHUMAZ[18]) (Figures 11 and S5C), no hydrogen-bonding pattern is present between columns synthons. Here, only sterical hindrance between prolinium ions is a guide for organization of columns and therefore organization of the structure itself, with coformer molecules grafted to the columns and without any molecular interactions between them.

Conformational Analysis by Quantum Mechanics Calculation. The conformation of the prolinium zwitterion has been approached by theoretical methods and a systematic conformational scan around torsion angle T has been performed (Figure 12). The scan presents two conformations that are the most stable: $T = 0°$ and 180°. Values of T observed among the structures obtained in the present work and in those retrieved from the CSD do correspond to stable conformations determined by the conformational scan (Figure 12).

The ability of proline to disrupt the carboxylic acids homosynthon hydrogen bonds (as evoked in Point 2.3) can in part be explained by a possible gain of charge residing on its formally negatively charged oxygen atom, evidently owing to its zwitterionic nature. This would give rise to a more stable (heterosynthon) hydrogen bond than the one formed between the neutral COOH carboxylic acid groups of fumaric acid. To quantify this effect, electronic charges on the hydrogen-bond donors and acceptors have been calculated on the experimental structure of L-prolinium/fumaric acid coming from our SCXRD analysis (Figure 13). Determination of relative energies for hydrogen-bonding patterns between prolinium and fumaric acid in the crystallographic structure has also been estimated, using the electrostatic potential representation for each entity (Figure 13). The difference in energy ($\Delta E = E(Pro^{\pm}–Fum) – [E(Pro^{\pm}) + E(Fum)]$) between the two partners involved in a heterosynthon hydrogen bond ($E(Pro^{\pm}–Fum)$), and the energy of the prolinium ($E(Pro^{\pm})$) and the fumaric acid ($E(Fum)$) alone in the structure, is around 15−17 kJ/mol in favor of the hydrogen bond coformers. Energy values for hydrogen bond patterns have been performed by calculations on isolated molecular pairs and with molecular conformations directly coming from the crystal structure. While this approach

dx.doi.org/10.1021/cg400081v | Cryst. Growth Des. 2013, 13, 2373−2389

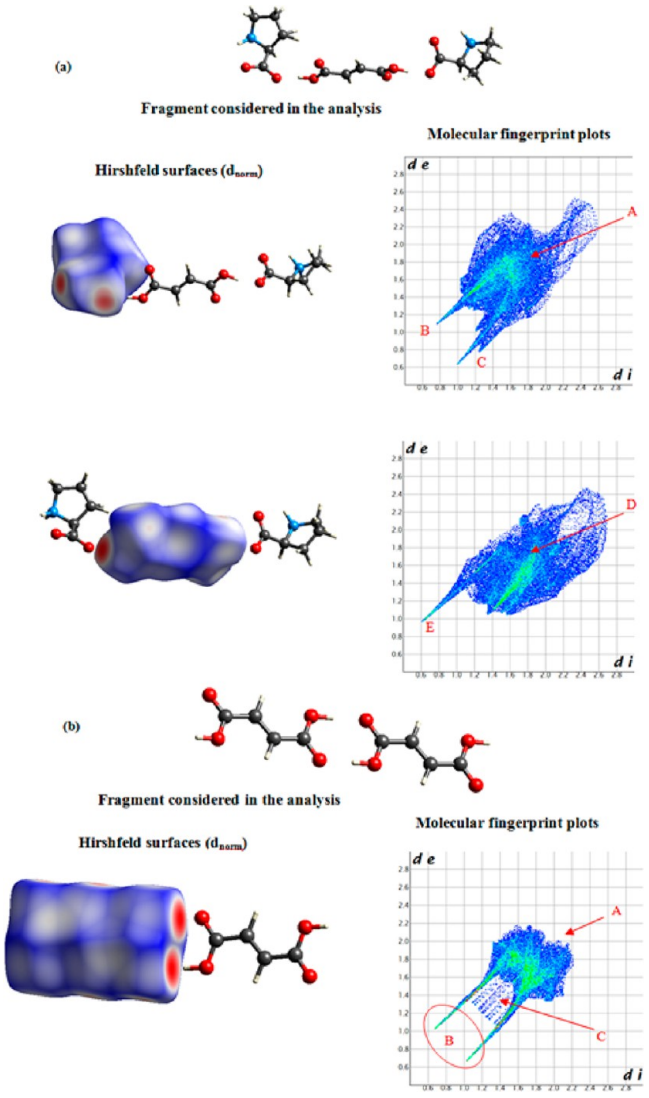

Figure 14. (a) Hirshfeld surfaces and molecular fingerprints for H-bonds heterosynthon between L-prolinium and fumaric acid considered for theoretical relative energy determination of the two H-bonds implicated in the multimolecular fragment (A: No stacking interactions, B: O--H H-bonding interaction with donor on the upper spike and acceptor on the down spike, C: Other less pronounced H-bonds types on the immediate neighboring of the prolinium, D: No stacking interactions but more long-distance interactions present here than for prolinium, E: O--H H-bonding interaction, clearly donor on the upper spike) and (b) Hirshfeld surfaces and molecular fingerprints for H-bonds homosynthon between fumaric acid molecules in the monoclinic structure (A: Many less long-distance interaction than for situation in (a), B: Very strong O--H H-bonding interaction with donor on the upper side and acceptor on the down spike, C: Typical behavior from cyclic H-bonds).

furnishes helpful information on the stabilization energy of the system, a more realistic approach performed by taking into account the effects of molecular packing could be realized. But for this purpose, much more computationally expensive methodologies (e.g., DFT calculations with periodic boundaries conditions) would be needed. Mulliken sets of charges for the structure are also compared (Table 5), and as it can be deduced by the nature itself of the zwitterionic compound, negative charges on carboxylate moieties provoke a more pronounced ionic nature of the hydrogen bond (charge-assisted hydrogen bond) and favors formation of this heterosynthon interaction over the carboxylic homosynthon interactions between fumaric acid. In fact, homosynthon interactions between carboxylic groups arise in many cases when carboxylic acid are included in structures (33% of occurrence probability[57]) and lead to strong homodimers, that can be hard to break to form another synthon, especially when this is a less stable heterosynthon. But with a modification of the protonation state of the coformer (prolinium in our case) and a more pronounced ionic character in hydrogen-bond potential pattern, we forced a strong homodimer synthon to reorganize in different heterosynthons, with a global gain in energy.

From another point of view, Hirshfeld surface analysis[58−61] allows rationalization of the intermolecular interactions between each partner in the heterosynthon, by quantifying close contacts between elements in each L-prolinium/fumaric acid entity. Hirshfeld surfaces representations and decomposed molecular fingerprints are given in Figure 14. In each cocrystal, the global molecular fingerprint corresponds to a classical hydrogen bond behavior. L-Prolinium is both hydrogen-bond donor and acceptor, the acceptor behavior being more pronounced, as it can be seen from the spike down the fingerprint. Fumaric acid has a more pronounced hydrogen-bond donor character. In the case of L-prolinium, other hydrogen-bond interactions, less stable, can be noticed on the fingerprint plot as it has already been deduced before from the structure itself. These hydrogen bonds are the principal type of interaction present in the fragment considered here: for example, stacking interactions between neighboring molecules are absent. In comparison with the monoclinic crystal structure of fumaric acid, the hydrogen-bonding behavior of the fumaric acid molecule has been profoundly modified: the hydrogen-bond donor character has completely vanished, to take advantage of the hydrogen-bond acceptor character.

CONCLUSIONS

New zwitterionic cocrystals of L-proline, D-proline, and DL-proline with fumaric acid were obtained, which allowed a detailed study on these cocrystals (and salt compound implying prolinamide, a compound derived from proline). Analyses started with synthesis of the cocrystals by dry grinding, a simple and green method. Although residues of the pure starting compounds are traced in the ground product, the preparative method is efficient and well adapted for pharmaceutical derivatives. Single-crystal X-ray diffraction allowed the detailed study of the structure of the cocrystals and unambigously established the presence of proline under its zwitterionic form (prolinium, Pro$^{\pm}$) in all the structures. Cocrystal−cocrystal grinding of the chiral zwitterionic cocrystals (2:1 D-Pro$^{\pm}$−Fum +2:1 L-Pro$^{\pm}$−Fum) produced the racemic three-component cocrystal of DL-proline and fumaric acid (1:1:1 L-Pro$^{\pm}$−Fum−D-Pro$^{\pm}$). Alternatively, this compound can be partially obtained by dry grinding of the coformers, DL-proline and fumaric acid. Comparison with existing crystal structures implying the prolinium moiety provides general geometrical and organizational behavior for structures implying zwitterionic proline, that can be linked to the new structures produced in this work. Theoretical calculations have allowed determination of energetical (and charge) arguments in favor of formation of hetero H-bonds compared to strong dicarboxylic homosynthon interactions formed between two fumaric acid molecules, adding value to the formation of our new zwitterionic cocrystal structure. A detailed calorimetric analysis of L-prolinium/

dx.doi.org/10.1021/cg400081v | Cryst. Growth Des. 2013, 13, 2373−2389

fumaric acid cocrystal is now planned, in order to establish phase diagrams of the new zwitterionic structures formed in this work.

■ ASSOCIATED CONTENT

Supporting Information

Additional figures S1, S2, S3A, S3B, S3C, S3D, S3E, S4, S5A, S5B, S5C, and S5D and X-ray crystallographic information files (CIFs) for all original compounds in the study are available. This information is available free of charge via the Internet at http://pubs.acs.org.

■ AUTHOR INFORMATION

Corresponding Author

*Tel: +32 81 72 45 50. E-mail: johan.wouters@fundp.ac.be.

Notes

The authors declare no competing financial interest.

■ ACKNOWLEDGMENTS

A.T. thanks the "Fonds pour la formation à la Recherche dans l'Industrie et dans l'Agriculture" (FRIA) for its grant and support. Financial support of the FNRS (Grant No. 2.4511.07) is also acknowledged. Authors would like to thank Prof. Simon Cole and his staff in UK National Crystallography Service (Univ. of Southampton) for the data collection on structure DL-Pro/AF, Prof. Gérard Coquerel, and all his staff (especially Nicolas Couvrat, Ph.D.) in SMS laboratory, at the University of Rouen (France) for DSC measurements and Dr. Luc Quéré for continuous interest in this work.

■ ABBREVIATIONS

SCXRD, single-crystal X-ray diffraction; XRPD, X-ray powder diffraction; DFT, density functional theory; DSC, differential scanning calorimetry; Pro, proline, Fum, fumaric acid

■ REFERENCES

(1) Trask, A. V.; Motherwell, W. D. S.; Jones, W. *Int. J. Pharm.* **2006**, *320*, 114−123.
(2) Serajuddin, A. T. M. *J. Pharm. Sci.* **1999**, *88*, 1058−1066.
(3) Berge, S. M.; Bighley, L. D.; Monkhouse, D. C. *J. Pharm. Sci.* **1977**, *66*, 1−19.
(4) Basavoju, S.; Boström, D.; Velaga, S. P. *Pharm. Res.* **2008**, *25* (3), 530−541.
(5) Wermuth, C. G.; Stahl, P. H. In *Handbook of Pharmaceutical Salts: Properties, Selection and Use*; Stahl, P. H., Wermuth, C. G., Eds.; VHCA, Verlag Helvetica Chimica Acta: Zürich, Switzerland and Wiley-VCH, Verlag GmbH & Co. KGaA: Weinheim, Germany, 2002; IUPAC Series, Introduction, pp 1−9.
(6) Bighley, L. D.; Berge, S. M.; Monkhouse, D. C. In *Encyclopedia of Pharmaceutical Technology*; Swarbrick, J.; Boylan, J. C., Eds.; M. Dekker Inc.: New York, 1996; Vol. *15*, Chapter 2, pp 19−34.
(7) Kaushal, A. M.; Gupta, P.; Bansal, A. K. *Crit. Rev. Ther. Drug Carrier Syst.* **2004**, *21*, 133−193.
(8) McNamara, D. P; Childs, S. L.; Giordano, J.; Iarricio, A.; Cassidy, J.; Shet, M. S.; Mannion, R.; O'Donnell, E.; Park, A. *Pharm. Res.* **2006**, *23*, 1888−1897.
(9) Wouters, J.; Tilborg, A.; Quéré, L. In *Pharmaceuticals Salts and Cocrystals*; Wouters, J., Quéré, L., Eds.; Royal Society of Chemistry Publishing: Cambridge, UK, 2012; RSC Drug Discovery Series 16, Chapter 15, pp 330−337.
(10) Shan, N.; Zaworotko, M. J. *Drug Discovery Today* **2008**, *13*, 440−446.
(11) Bhatt, P. M.; Azim, Y.; Thakur, T. S.; Desiraju, G. R. *Cryst. Growth Des.* **2009**, *9*, 951−957.
(12) Basajovu, S.; Boström, B.; Velaga, S. P. *Cryst. Growth Des.* **2006**, *6*, 2699−2708.
(13) Shiraki, K.; Takata, N.; Takano, R.; Hayashi, Y.; Terada, K. *Pharm. Res.* **2008**, *25*, 2581−2592.
(14) Good, D. J.; Rodríguez-Hornedo, N. *Cryst. Growth Des.* **2009**, *9*, 2252−2264.
(15) Blagden, N.; de Matas, M.; Gavan, P. T.; York, P. *Adv. Drug Delivery Rev.* **2007**, *59*, 617−630.
(16) Sridhar Prasad, G.; Vijayan, M. *Acta Crystallogr., Sect. B: Struct. Crystallogr. Cryst. Chem.* **1993**, *49*, 348−356.
(17) Aakeroy, C. B.; Bahra, G. S.; Brown, C. R.; Hitchcock, P. B.; Patell, Y.; Seddon, K. R. *Acta Chem. Scand.* **1995**, *49*, 762−767.
(18) Timofeeva, T. V.; Kuhn, G. H.; Nesterov, V. V.; Nesterov, V. N.; Frazier, D. O.; Penn, B. G.; Antipin, M.Yu. *Cryst.Growth Des.* **2003**, *3*, 383−391.
(19) Qu, X.; Lu, J.; Zhao, C.; Boas, J. F.; Moubaraki, B.; Murray, K. S.; Siriwardana, A.; Bond, A. M.; Martin, L. L. *Angew. Chem., Int. Ed.*. **2011**, *50* (7), 1589−1592.
(20) Klussmann, M.; Iwamura, H.; Mathew, S. P.; Wells, D. H., Jr; Pandya, U.; Armstrong, A.; Blackmond, D. G. *Nature Lett.* **2006**, *441*, 621−623.
(21) Zotova, N.; Broadbelt, L. J.; Armstrong, A.; Blackmond, D. G. *Bioorg. Med. Chem. Lett.* **2009**, 3934−3937.
(22) Blackmond, D. G.; Moran, A.; Hughes, M.; Armstrong, A. *J. Am. Chem. Soc.* **2010**, *132*, 7598−7599.
(23) Donnay, J. D. H.; Harker, D. *Am. Mineral.* **1937**, *22*, 446−447.
(24) *Mercury CSD 2.0* - New Features for the Visualization and Investigation of Crystal Structures. Macrae, C. F.; Bruno, I. J.; Chisholm, J. A.; Edgington, P. R.; McCabe, P.; Pidcock, E.; Rodriguez-Monge, L.; Taylor, R.; van de Streek, J.; Wood, P. A. *J. Appl. Crystallogr.* **2008**, *41*, 466-470.
(25) Bruno, I. J.; Cole, J. C.; Edgington, P. R.; Kessler, M.; Macrae, C. F.; McCabe, P.; Pearson, J.; Taylor, R. *Acta Crystallogr., Sect. B: Struct. Crystallogr. Cryst. Chem.* **2002**, *58*, 389−397.
(26) *CCDC. Vista - A Program for the Analysis and Display of Data Retrieved from the CSD*; Cambridge Crystallographic Data Centre, Cambridge, England, 1994.
(27) Adamo, C.; Barone, V. *J. Chem. Phys.* **1999**, *110*, 6158−6170.
(28) Adamo, C.; Scuseria, G. E.; Barone, V. *J. Chem. Phys.* **1999**, *111*, 2889−2899.
(29) Ernzerhof, M.; Scuseria, G. E. *J. Chem. Phys.* **1999**, *110*, 5029−5036.
(30) *Gaussian 09*, Revision A.1; Frisch, M. J.; Trucks, G. W.; Schlegel, H. B.; Scuseria, G. E.; Robb, M. A.; Cheeseman, J. R.; Scalmani, G.; Barone, V.; Mennucci, B.; Petersson, G. A.; Nakatsuji, H.; Caricato, M.; Li, X.; Hratchian, H. P.; Izmaylov, A. F.; Bloino, J.; Zheng, G.; Sonnenberg, J. L.; Hada, M.; Ehara, M.; Toyota, K.; Fukuda, R.; Hasegawa, J.; Ishida, M.; Nakajima, T.; Honda, Y.; Kitao, O.; Nakai, H.; Vreven, T.; Montgomery, Jr., J. A.; Peralta, J. E.; Ogliaro, F.; Bearpark, M.; Heyd, J. J.; Brothers, E.; Kudin, K. N.; Staroverov, V. N.; Kobayashi, R.; Normand, J.; Raghavachari, K.; Rendell, A.; Burant, J. C.; Iyengar, S. S.; Tomasi, J.; Cossi, M.; Rega, N.; Millam, J. M.; Klene, M.; Knox, J. E.; Cross, J. B.; Bakken, V.; Adamo, C.; Jaramillo, J.; Gomperts, R.; Stratmann, R. E.; Yazyev, O.; Austin, A. J.; Cammi, R.; Pomelli, C.; Ochterski, J. W.; Martin, R. L.; Morokuma, K.; Zakrzewski, V. G.; Voth, G. A.; Salvador, P.; Dannenberg, J. J.; Dapprich, S.; Daniels, A. D.; Farkas, Ö.; Foresman, J. B.; Ortiz, J. V.; Cioslowski, J.; Fox, D. J. Gaussian, Inc.: Wallingford, CT, 2009.
(31) Wolff, S. K.; Grimwood, D. J.; McKinnon, J. J.; Turner, M. J.; Jayatilaka, D.; Spackman, M. A. *CrystalExplorer*, Version 3.0; University of Western Australia, 2012.
(32) Friščić, T.; Jones, W. *Cryst. Growth Des.* **2009**, *9* (3), 1621−1637.
(33) Rehder, S.; Klukkert, M.; Löbmann, K. A. M.; Strachan, C. J.; Sakmann, A.; Gordon, K.; Rades, T.; Leopold, C. S. *Pharmaceutics* **2011**, *3*, 706−722.
(34) Nguyen, K. L.; Friščić, T.; Day, M. G.; Gladden, L. F.; Jones, W. *Nat. Mater.* **2007**, *6*, 206−209.
(35) Schmuttenmaer, C. A. *Chem. Rev.* **2004**, *104*, 1759−1779.

(36) Gillard, R. D.; Irving, H. M.; Parkins, R. M.; Payne, N. C.; Pettit, L. D. *J. Chem. Soc. A* **1966**, 1159.
(37) Dahlgren, G.; Long, F. A. *J. Am. Chem. Soc.* **1960**, *82*, 1303−1308.
(38) Childs, S. L.; Stahly, G. P.; Park, A. *Mol. Pharmaceutics* **2007**, *4* (3), 323−338.
(39) Marchand, A. P.; Watson, W. H., *Private Communication to the Cambridge Sructural Database*, 2006, deposition number CCDC623459.
(40) Jeffrey, G. A. In *An Introduction to Hydrogen Bonding*; Oxford University Press Inc.: New York, USA, 1997; Chapter 2, pp 11−32.
(41) Allen, F. H. *Acta Crystallogr., Sect. B: Struct. Crystallogr. Cryst. Chem.* **2002**, *58*, 380−388.
(42) Brown, C. J. *Acta Crystallogr., Sect. E: Struct. Rep. Online* **1966**, *21*, 1.
(43) Yardley, K. *J.Chem.Soc.* **1925**, *127*, 2207.
(44) Bednowitz, A. L.; Post, B. *Acta Crystallogr., Sect. E: Struct. Rep. Online* **1966**, *21*, 566.
(45) Roldan, L. G.; Rahl, F. J.; Paterson, A. R. *Acta Crystallogr., Sect. E: Struct. Rep. Online* **1965**, *19*, 1055.
(46) Sridhar Prasad, G.; Vijayan, M. *Acta Crystallogr., Sect. B: Struct. Crystallogr. Cryst. Chem.* **1993**, *49*, 348−349.
(47) Takata, N.; Shiraki, K.; Takano, R.; Hayashi, Y.; Terada, K. *Cryst. Growth Des.* **2008**, *8* (8), 3032−3037.
(48) Schultheiss, N.; Newman, A. *Cryst. Growth Des.* **2009**, *9* (6), 2950−2967.
(49) Temesvári, I.; G. Liptay, G.; Pungor, E. *J. Therm. Anal.* **1971**, *3*, 293−295.
(50) Friščić, T.; Fábián, L.; Burley, J. C.; Jones, W.; Motherwell, W. D. S. *Chem. Commun.* **2006**, 5009−5011.
(51) Braga, D.; Grepioni, F.; Lampronti, G. I. *CrystEngComm* **2011**, *13*, 3122−3124.
(52) Tilborg, A.; Springuel, G.; Norberg, B.; Wouters, J.; Leyssens, T. *CrystEngComm* **2013**, *15* (17), 3341−3350.
(53) Kayushina, R. L.; Vainshtein, B. K. *Crystallogr. Rep.* **1965**, *10*, 833−844.
(54) Myung, S.; Pink, M.; Baik, M. H.; Clemmer, D. E. *Acta Crystallogr., Sect. C: Cryst. Struct. Commun.* **2005**, *61*, o506−o508.
(55) Muramulla, S.; Arman, H. D.; Zhao, C. G.; Tiekink, E. R. T. *Acta Crystallogr., Sect. E: Struct. Rep. Online* **2009**, *65*, o3070.
(56) Athimoolam, S.; Natarajan, S. *Acta Crystallogr., Sect. C: Cryst. Struct. Commun.* **2007**, *63*, o283.
(57) Allen, F. H.; Motherwell, W. D. S.; Raithby, P. R.; Shields, G. P.; Taylor, R. *New. J. Chem.* **1999**, 23−25.
(58) Spackman, M. A.; McKinnon, J. J. *CrystEngComm* **2002**, *4* (66), 378−392.
(59) McKinnon, J. J.; Spackman, M. A.; Mitchell, A. S. *Acta Crystallogr., Sect. B: Struct. Crystallogr. Cryst. Chem.* **2004**, *60*, 627−668.
(60) McKinnon, J. J.; Jayatilaka, D.; Spackman, M. A. *Chem. Commun.* **2007**, 3814−3816.
(61) McKinnon, J. J.; Jayatilaka, D. *CrystEngComm* **2009**, *11*, 19−32.
(62) Gharzaryan, V. V.; Fleck, M.; Petrosyan. *Proc. SPIE* **2011**, *7998*, 79980.
(63) Ramanathan, C. R.; Periasamy, M. *Tetrahedron: Asymmetry* **1998**, *9*, 2651−2656.
(64) Pandiarajan, S.; Sridhar, B.; Rajaram, R. K. *Acta Crystallogr., Sect. E: Struct. Rep. Online* **2002**, *58*, o74−o76.
(65) Rogowska, P.; Cyranski, M. K.; Sporzynski, A.; Ciesielski, A. *Tetrahedron Lett.* **2006**, *47*, 1389−1393.
(66) Pandiarajan, S.; Sridhar, B.; Rajaram, R. K. *Acta Crystallogr., Sect. E: Struct. Rep. Online* **2002**, *58*, o1370−o1371.
(67) Fu, T. Y.; Scheffer, J. R.; Trotter, J. *Acta Crystallogr., Sect. C: Cryst. Struct. Commun.* **1997**, *53*, 1257−1259.